The Astrophysical Journal Supplement Series, 247:1 (25pp), 2020 March https://doi.org/10.3847/1538-4365/ab67b6

Superhydrogenated Polycyclic Aromatic Hydrocarbon Molecules: Vibrational Spectra in the Infrared

X. J. Yang[1,2], Aigen Li[2], and R. Glaser[3]
[1] Department of Physics, Xiangtan University, 411105 Xiangtan, Hunan Province, People's Republic of China; xjyang@xtu.edu.cn
[2] Department of Physics and Astronomy, University of Missouri, Columbia, MO 65211, USA; lia@missouri.edu
[3] Department of Chemistry, University of Missouri, Columbia, MO 65211, USA; glaserr@missouri.edu
Received 2019 October 6; revised 2019 December 10; accepted 2019 December 31; published 2020 February 20

Abstract

Superhydrogenated polycyclic aromatic hydrocarbons (PAHs) may be present in H-rich and ultraviolet-poor benign regions. The addition of excess H atoms to PAHs converts the aromatic bonds into aliphatic bonds, the strongest of which falls near 3.4 μm. Therefore, superhydrogenated PAHs are often hypothesized to be a carrier of the 3.4 μm emission feature that typically accompanies the stronger 3.3 μm aromatic C–H stretching feature. To assess this hypothesis, we use density function theory to compute the infrared (IR) vibrational spectra of superhydrogenated PAHs and their ions of various sizes (ranging from benzene and naphthalene to perylene and coronene) and of various degrees of hydrogenation. For each molecule, we derive the intrinsic oscillator strengths of the 3.3 μm aromatic C–H stretch ($A_{3.3}$) and the 3.4 μm aliphatic C–H stretch ($A_{3.4}$). By comparing the computationally derived mean ratio of $\langle A_{3.4}/A_{3.3}\rangle \approx 1.98$ with the mean ratio of the observed intensities $\langle I_{3.4}/I_{3.3}\rangle \approx 0.12$, we find that the degree of superhydrogenation—the fraction of carbon atoms attached with extra hydrogen atoms—is only ~2.2% for neutral PAHs, which predominantly emit the 3.3 and 3.4 μm features. We also determine for each molecule the intrinsic band strengths of the 6.2 μm aromatic C–C stretch ($A_{6.2}$) and the 6.85 μm aliphatic C–H deformation ($A_{6.85}$). We derive the degree of superhydrogenation from the mean ratio of the observed intensities $\langle I_{6.85}/I_{6.2}\rangle \lesssim 0.10$ and $\langle A_{6.85}/A_{6.2}\rangle \approx 1.53$ for neutrals and $\langle A_{6.85}/A_{6.2}\rangle \approx 0.56$ for cations to be $\lesssim$3.1% for neutrals and $\lesssim$8.6% for cations. We conclude that astrophysical PAHs are primarily aromatic and are only marginally superhydrogenated.

Unified Astronomy Thesaurus concepts: Polycyclic aromatic hydrocarbons (1280); Interstellar line emission (844); Line intensities (2084)

1. Introduction

The so-called "unidentified" infrared (IR) emission (UIE) bands, which are composed of a distinctive set of broad emission features at 3.3, 6.2, 7.8, 8.6, and 11.3 μm, are ubiquitously detected in a wide range of Galactic and extragalactic environments (see Tielens 2008). The hypothesis of polycyclic aromatic hydrocarbon (PAH) molecules as a viable carrier of the UIE bands, originally proposed by Léger & Puget (1984), and Allamandola et al. (1985), has been widely accepted. The PAH hypothesis attributes the UIE bands to the vibrational modes of PAHs, with the 3.3 μm feature assigned to C–H stretching modes, the 6.2 and 7.7 μm features to C–C stretching modes, the 8.6 μm feature to C–H in-plane bending modes, and the 11.3 μm feature to C–H out-of-plane bending modes. According to this hypothesis, PAHs are present in the interstellar medium (ISM) in various sizes, geometries, and charging states (Allamandola et al. 1989; Peeters et al. 2004). The relative strengths of these bands depend on the size, charge and molecular structure of the PAH molecule (Allamandola et al. 1999; Draine & Li 2001) and the physical conditions (e.g., the intensity and hardness of the starlight illuminating the molecule, the electron density, and gas temperature; see Bakes & Tielens 1994; Weingartner & Draine 2001).

In the diffuse ISM and photodissociated regions (PDRs) where hydrogen (H) atoms are abundant, astronomical PAHs are exposed to the continuous bombardment of H atoms and may likely have excess peripheral H atoms (see Andrews et al. 2016 and references therein). In the following, we designate superhydrogenated PAHs as those PAHs whose edges contain excess H atoms. In the literature, superhydrogenated PAHs are often also called hydrogenated PAHs. In this work we will use the term "superhydrogenated PAHs" (or "superhydrogenation") interchangeably used with the term "hydrogenated PAHs" (or "hydrogenation"). The interaction between PAHs and H atoms has been studied both theoretically (Cassam-Chenaï et al. 1994; Bauschlicher 1998; Le Page et al. 2009) and experimentally (Ricks et al. 2009; Boschman et al. 2012; Klærke et al. 2013; Cazaux et al. 2016). These studies have demonstrated that it is possible to superhydrogenate PAH cations, particularly in regions rich in ultraviolet (UV) photons (e.g., the surface of PDRs). Theoretical studies have also shown that superhydrogenation of neutral PAHs in H-rich, UV-poor benign regions (e.g., protoplanetary nebulae) is possible (e.g., see Rauls & Hornekær 2008; Rasmussen et al. 2011). Experimentally, it has been demonstrated that coronene ($C_{24}H_{12}$) could be fully superhydrogenated to form perhydrocoronene ($C_{24}H_{36}$) in low UV flux regions (see Thrower et al. 2012, 2014). Wolf et al. (2016) explored experimentally the photostability of cationic pyrene ($C_{16}H_{10}^{+}$) with six ($C_{16}H_{16}^{+}$) or 16 extra H atoms ($C_{16}H_{26}^{+}$) and found superhydrogenated pryene cations would undergo backbone fragmentation upon absorption of two (for $C_{16}H_{16}^{+}$) or one (for $C_{16}H_{26}^{+}$) photons of energy just below 3 eV. On the other hand, by combining thermal desorption mass spectrometry measurements and density functional theory (DFT) calculations, Jensen et al. (2019) have shown the existence of stable configurations of superhydrogenated neutral coronene. Halasinski et al. (2005) and Hammonds et al. (2009) obtained the electronic spectra of hydrogenated PAHs and their ions, respectively through the matrix isolation spectroscopy experiments and the time-dependent DFT computations. They argued that hydrogenated PAHs might be responsible for some of the diffuse interstellar bands.

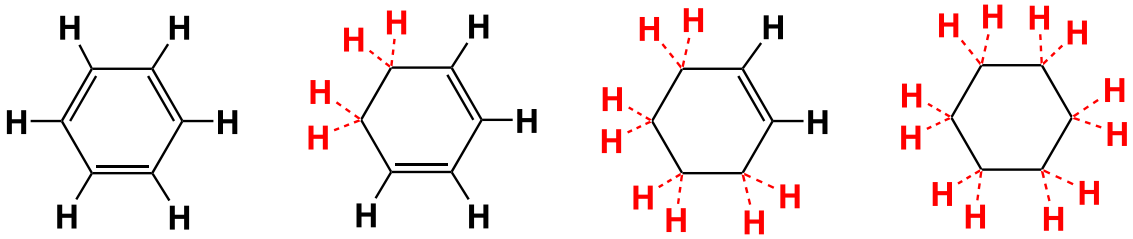

Figure 1. Structures of benzene and hydrogenated benzenes.

Superhydrogenated PAHs have been suggested to be (at least partly) responsible for the 3.4 μm emission feature detected in many UIE sources, which always accompanies the (often much stronger) 3.3 μm feature (e.g., see Geballe et al. 1985, 1989; Jourdain de Muizon et al. 1986, 1990; Nagata et al. 1988; Allamandola et al. 1989; Sandford 1991; Sandford et al. 1991; Joblin et al. 1996; Sloan et al. 1997; Goto et al. 2003; Smith et al. 2004; Kondo et al. 2012; Yamagishi et al. 2012; Seok & Li 2017; Quitián-Lara et al. 2018). The exact carrier of the 3.4 μm emission feature remains unidentified, although it is often thought to arise from the aliphatic side chains attached as functional groups to PAHs (see Yang et al. 2017a and references therein). However, Wagner et al. (2000) obtained the IR emission spectra of five gas-phase UV laser-excited PAHs, two of which are methylated and three of which are peripherally hydrogenated. They found that hydrogenated PAHs produce a better match to astrophysical data than methylated PAHs. The 3.4 μm emission feature could also be due to the anharmonicity of the aromatic C–H stretching vibration (see Barker et al. 1987; Maltseva et al. 2016). Let v be the vibrational quantum number. In a harmonic oscillator, the spacing between all adjacent vibrational energy levels is constant, hence the $\Delta v = 1$ vibrational transitions between high v levels result in the same spectral line as that of the $v = 1 \rightarrow 0$ transition. In contrast, anharmonicity would continuously decrease the spacing between the adjacent vibrational states for higher values of v, and therefore the $\Delta v = 1$ transitions between higher v levels occur at increasingly longer wavelengths. The anharmonicity model interprets the weaker feature at 3.4 μm as the $v = 2 \rightarrow 1$ "hot band" of the 3.3 μm fundamental $v = 1 \rightarrow 0$ aromatic C–H stretching mode (see Barker et al. 1987).[4]

In superhydrogenated PAHs, some peripheral C atoms have two H atoms and the extra H atom converts the originally aromatic ring into an aliphatic ring. This creates two aliphatic C–H stretching bands: one due to the symmetric and the other to the asymmetric C–H stretching modes. These bands would fall near 3.4 μm and could (at least partly) account for the 3.4 μm emission (Schutte et al. 1993; Bernstein et al. 1996; Sandford et al. 2013; Steglich et al. 2013). Pauzat & Ellinger (2001) suggested that hydrogenated PAHs also produce series of bands that may be at the origin of the broad plateau observed below the 3.4 μm feature.

Superhydrogenated PAHs also exhibit two aliphatic C–H deformation bands at ~6.85 and 7.25 μm (e.g., see Sandford et al. 2013). Their low intensities put them at the limit of modern observational techniques. Observationally, these two bands have been detected both in the Milky Way and in the Large and Small Magellanic Clouds (e.g., see Acke et al. 2010; Sloan et al. 2014; Materese et al. 2017), but only in a limited number of objects (see Table 3 of Yang et al. 2016a for a summary). This will change with the launch of the *James Webb Space Telescope* (*JWST*). The Mid-IR Instrument (MIRI) on *JWST* will cover the wavelength range of the aliphatic C–H deformation bands with a medium spectral resolution of ~1550–3250 and unprecedented sensitivity. On the other hand, the Near-IR Spectrograph (NIRSpec) on *JWST*, with a spectral resolution up to ~2700, will allow probing of the aromatic and aliphatic C–H stretches at 3.3 and 3.4 μm in depth. *JWST*'s unique high sensitivity and near- and mid-IR medium spectral resolution capabilities will open up an IR window unexplored by the *Spitzer Space Telescope* and unmatched by the *Infrared Space Observatory* (*ISO*) and thus will probably place the detection of superhydrogenated PAHs on firm ground and enable far more detailed band analysis than previously possible.

The opportunity to thoroughly probe superhydorgenated PAHs in various astrophysical regions using *JWST* motivates us to employ DFT to compute the IR spectra of a series of superhydrogenated PAH molecules and their cations, with special attention paid to the intrinsic strengths of the aliphatic C–H bands at 3.4, 6.85, and 7.25 μm. In Section 2 we briefly describe the computational methods and the structures of our target molecules. Section 3 presents the computed IR spectra, as well as the intrinsic oscillator strengths of the aromatic and aliphatic C–H bands. The astrophysical implications are discussed in Section 4. Finally, we summarize our major results in Section 5.

2. Computational Methods and Target Molecules

We use the software Gaussian09 and Gaussian16 (Frisch et al. 2009) to calculate the IR vibrational spectra of a range of superhydrogenated PAHs and their cations. We employ the hybrid DFT method B3LYP (Frisch et al. 2009) in conjunction with the 6–311+G** basis set, i.e., triple ζ functions are included to describe the valence orbitals, diffuse functions are applied to the heavy (i.e., carbon) atoms, and polarization functions are applied to both heavy atoms and hydrogen atoms. The neutral hydrocarbons are closed-shell systems and they will be computed with restricted wave functions (RB3LYP). The cationic hydrocarbons are the result of single electron oxidation and these radical cations will be computed with unrestricted wave functions (UB3LYP). We optimize the molecule structures and then calculate the harmonic vibrational spectra (see Yang et al. 2017b and references therein).

Our target molecules include the derivatives of benzene (Figure 1), of naphthalene (Figure 2), of perylene (Figure 3),

[4] The anharmonicity model also predicts a weak band at ~1.6–1.8 μm, the overtone of the aromatic C–H stretch and/or combination bands (Brenner & Barker 1992; Geballe et al. 1994; Chen et al. 2019).

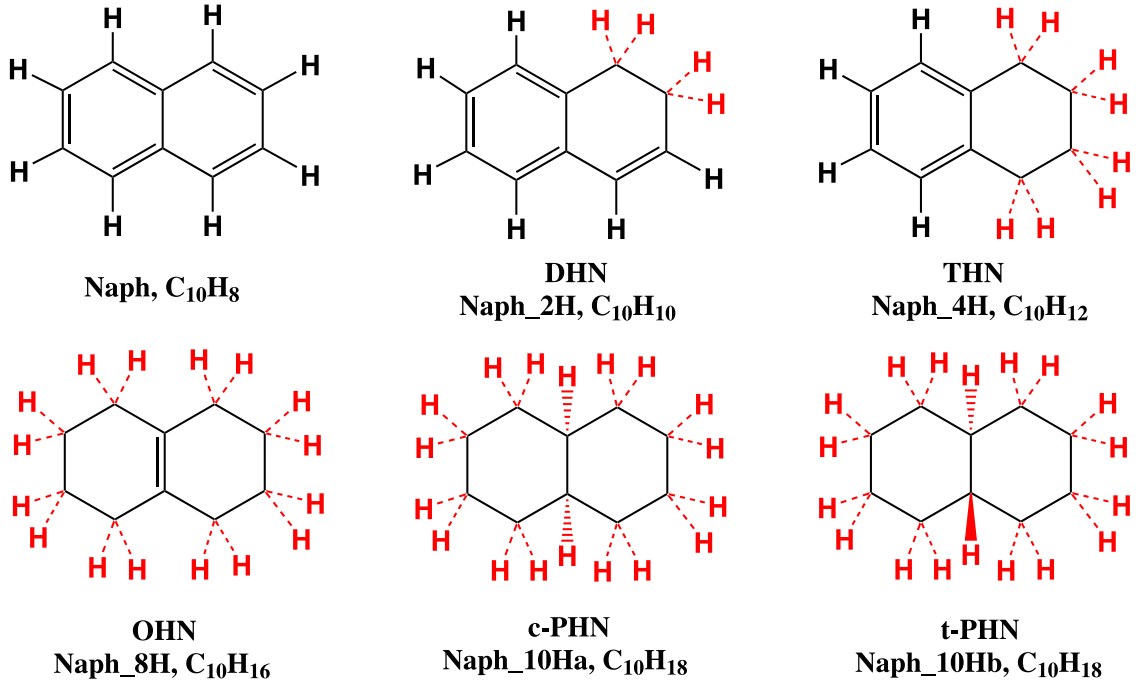

Figure 2. Structures of naphthalene and hydrogenated naphthalenes. The hydrogenated naphthalenes are labeled "Series A" in Sandford et al. (2013).

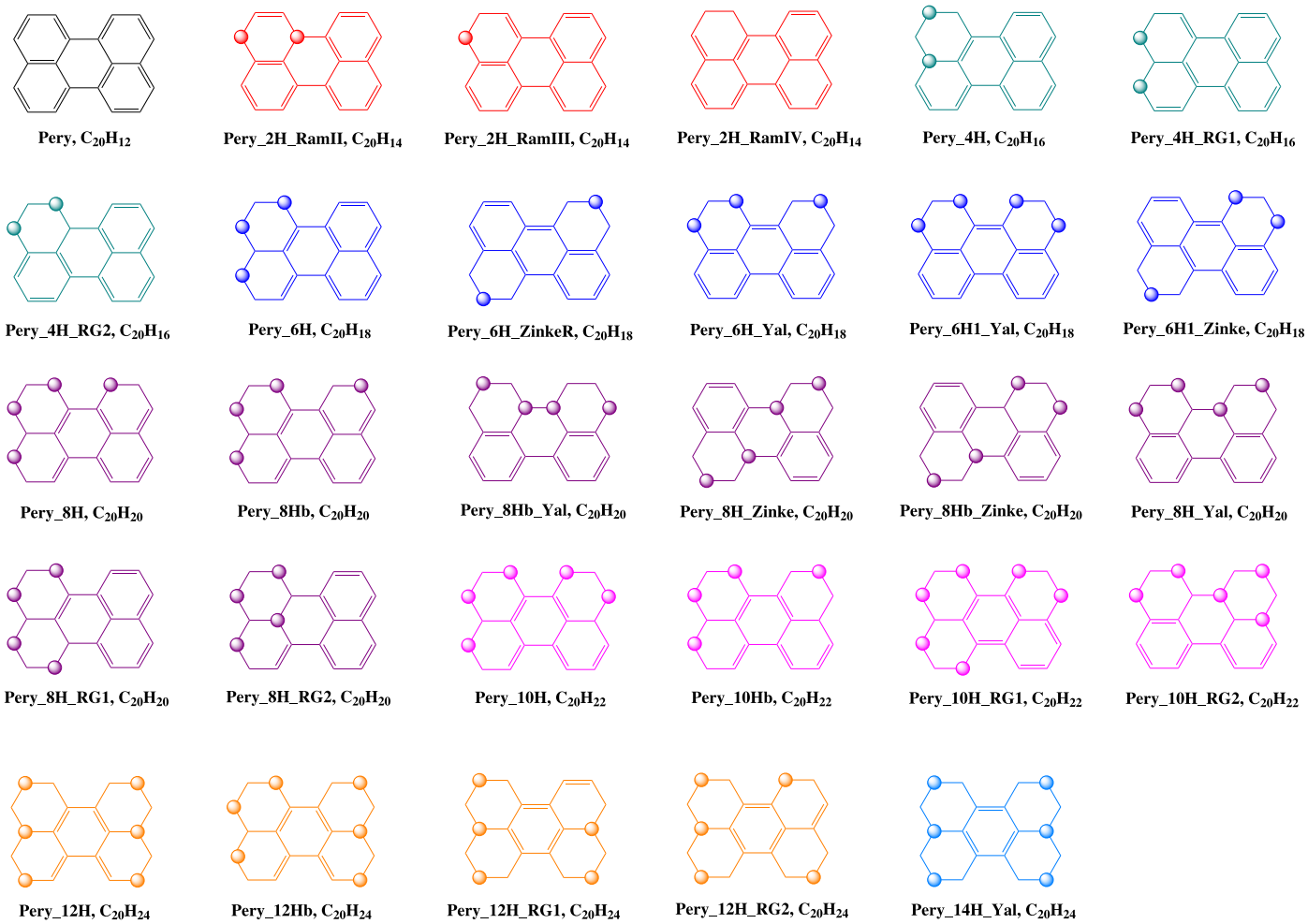

Figure 3. Structures of perylene and hydrogenated perylenes. All the molecules are named as follows: Pery plus the number of extra H atoms. The hydrogenated molecules are shown in different colors, with each color representing PAHs with the same number of extra H atoms.

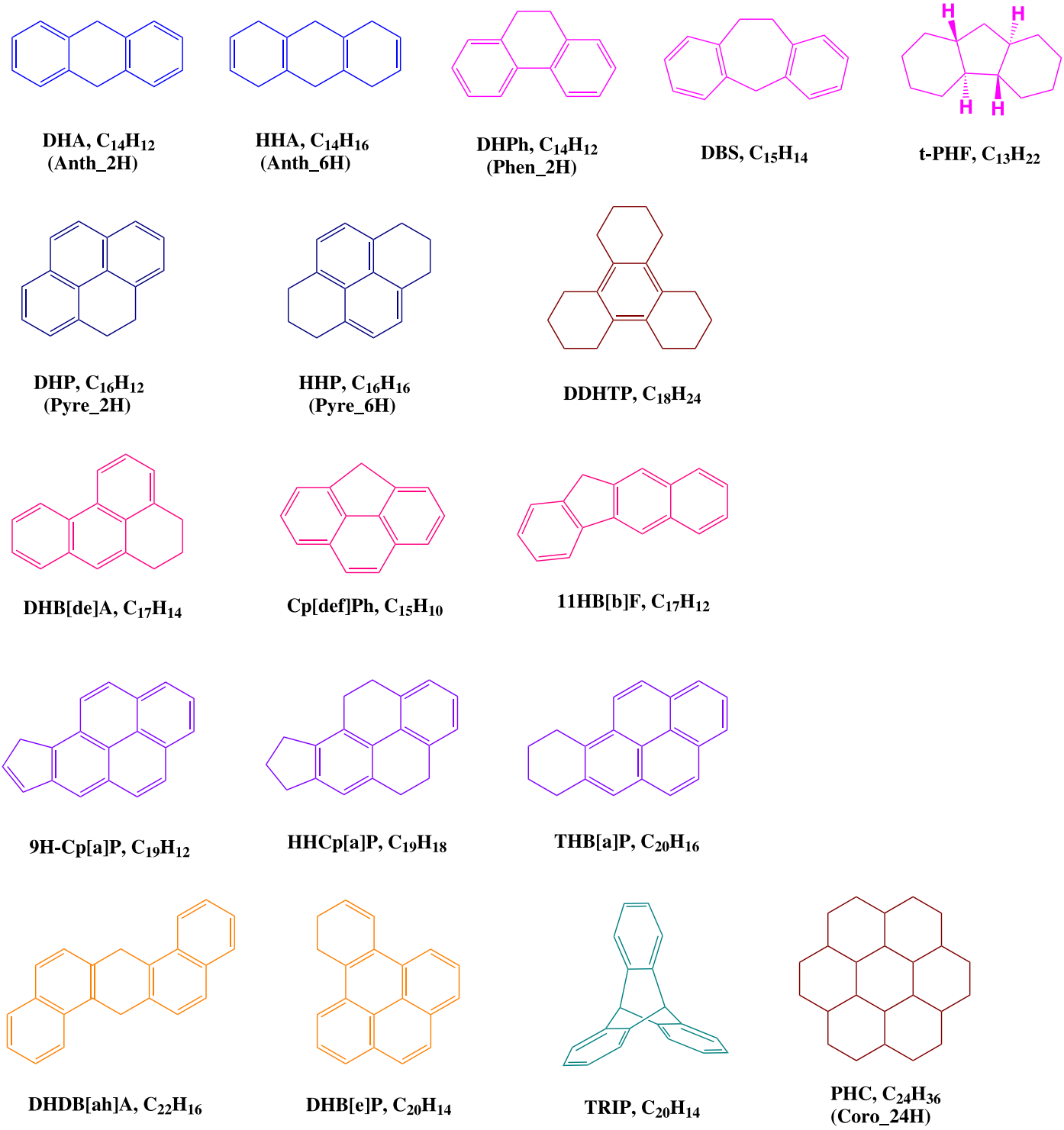

Figure 4. Structures of all the hydrogenated PAHs (except hydrogenated naphthalenes) experimentally studied by Sandford et al. (2013). These molecules were marked Series B, Series C, ..., and Series H in Sandford et al. (2013) and are shown here in different colors, with each color representing one series.

and of those experimentally investigated by Sandford et al. (2013; see Figure 4). For all our target molecules, we consider hydrogenation products that result from the addition of an even number of H atoms. The radical species resulting from the addition of an odd number of H atoms are likely to have short lifetimes. We will refer to hydrogenated species by the abbreviation of the first three or four letters of their parent PAH name followed by the number of extra H atoms (e.g., Pery_2H refers to perylene attached with 2 extra H atoms). But for those molecules studied by Sandford et al. (2013), we shall adopt the abbreviations given by them (see Table 1 of Sandford et al. 2013). More descriptive names shall also be used if such names are common. Many of the structures allow for structural isomers (i.e., H atoms are attached at different positions) and some of the structural isomers may adopt several conformations of the same connectivity but different spatial arrangements. Isomers and conformers will be distinguished by the addition of a letter.

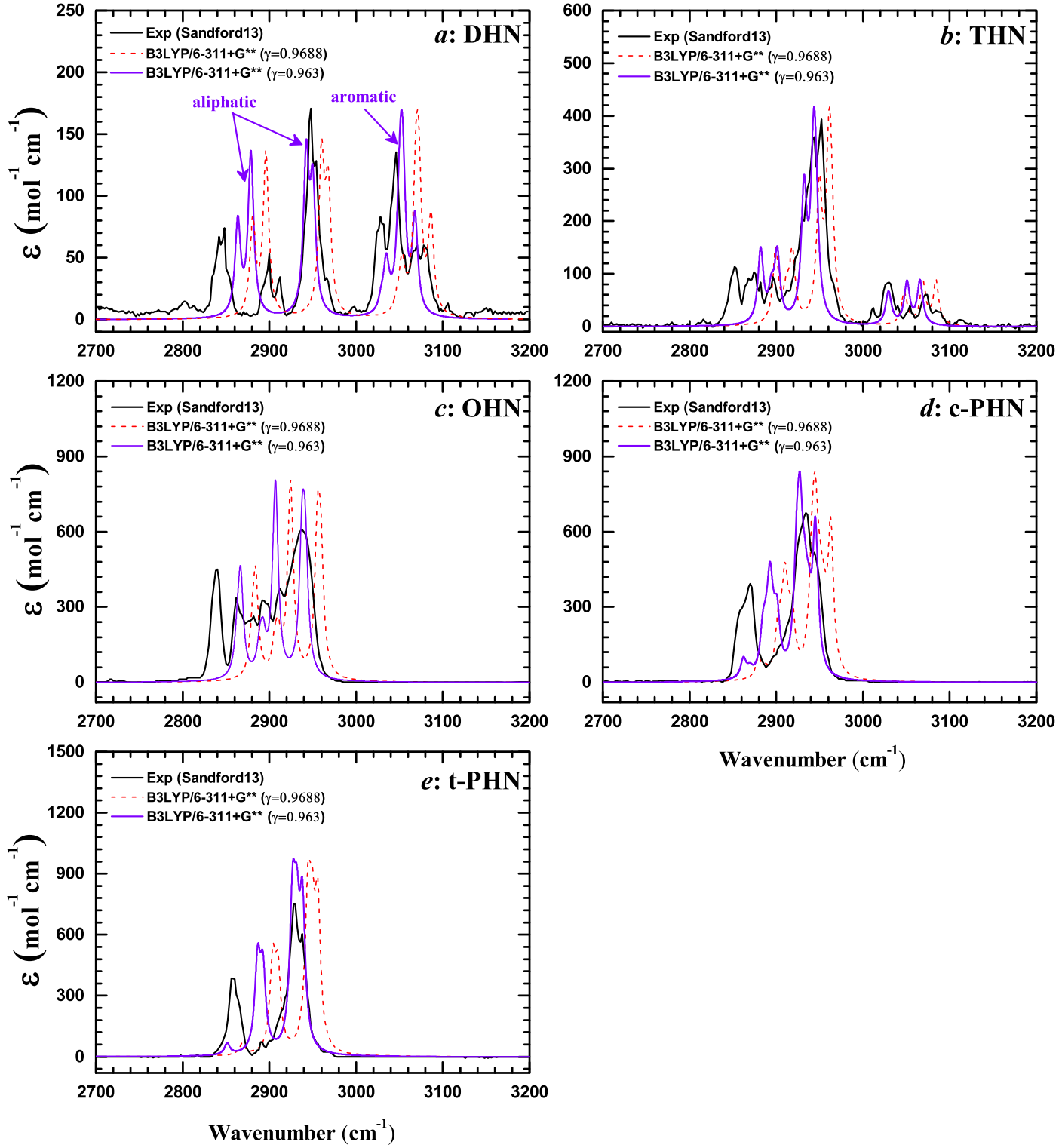

Figure 5. Comparison of the absorption spectra of hydrogenated naphthalenes computed at level B3LYP/6−311+G** with the experimental spectra of Sandford et al. (2013) [marked with "Exp(Sandford13)"]. We assign a line width of 4 cm^{-1} for the computed spectra. The frequencies of the computed spectra are multiplied by a scaling factor (γ) to be comparable with the experimental spectra (black solid lines). The red dashed lines are the computed spectra applied with $\gamma = 0.9688$ to the frequencies, and the purple solid lines are those applied with an optimized γ of 0.963. The band intensities—expressed as the molar absorption coefficient (ε) in units of $mol^{-1}\ cm^{-1}$ —of the experimental spectra are scaled to that of the computed spectra, since Sandford et al. (2013) did not measure the absolute band intensities. Note that in panel (a) for DHN, the 3.4 μm aliphatic C–H stretch consists of two complexes at ∼2870 cm^{-1} and ∼2950 cm^{-1}, while the 3.3 μm aromatic C–H stretch has only one complex at ∼3050 cm^{-1}.

In general, we will focus on the most likely and/or most stable structure. For benzene, for example, we will only consider cyclo–1,3–hexadiene (Ben_2H; see Figure 1), and ignore the less stable isomer cyclo–1,4–hexadiene. Also, we will consider only cyclohexene (Ben_4H; see Figure 1) and ignore all derivatives in which the CH groups are not geminal. Moreover, we will consider only the best conformation for all these systems, such as the chair conformation of cyclohexane (Ben_6H;

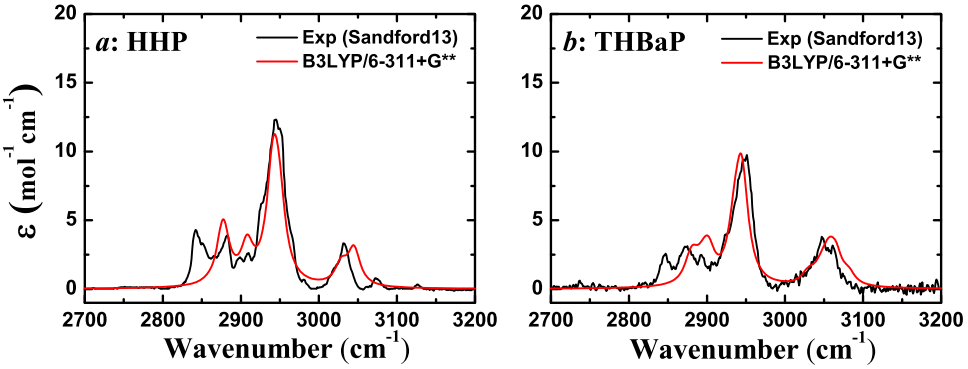

Figure 6. Comparison of the absorption spectra of HHP (i.e., Pyre_6H, $C_{16}H_{16}$; see Figure 4) and THB[a]P (i.e., $C_{20}H_{16}$; see Figure 4) computed at level B3LYP/6−311+G** with the experimental spectra of Sandford et al. (2013) [marked with "Exp(Sandford13)"]. To be comparable with the experimental spectra (black lines), the frequencies of the computed spectra (red lines) are multiplied by an optimized scaling factor of 0.963 and a line width of 10 cm^{-1} is assigned. The molar absorption coefficients ε of the experimental spectra are scaled to that of the computed spectra, since Sandford et al. (2013) did not measure the absolute band intensities.

Table 1
Computed Total Energies and Thermochemical Parameters for the Hydrogenated Benzene Molecules and Their Ions as Shown in Figure 1 at the B3LYP/6−311+G** Level

Compound	E_{tot}[a]	VZPE[b]	TE[c]	S[d]	ν_1[e]	ν_2[e]	μ[f]
Ben_2H	−233.483877	76.42	79.68	70.95	196.11	300.94	0.4992
Ben_4H	−234.713155	91.36	94.82	73.91	165.69	275.50	0.3573
Ben_6H	−235.944820	106.34	109.94	74.68	230.63	230.90	0.0000
Ben_2H+	−233.194323	75.78	79.23	74.30	95.51	250.66	0.0454
Ben_4H+	−234.394150	89.24	92.97	75.53	165.44	205.57	2.5497
Ben_6H+	−235.588818	101.51	105.63	78.71	198.63	261.93	0.0000

Notes.
[a] Total energies in atomic units.
[b] Vibrational zero-point energies (VZPE) in kcal mol^{-1}.
[c] Thermal energies (TE) in kcal mol^{-1}.
[d] Molecular entropies (S) in cal mol^{-1} K^{-1}.
[e] The lowest vibrational modes ν_1 and ν_2 in cm^{-1}.
[f] Dipole moment in Debye.

see Figure 1), while ignoring the less stable boat conformations. For dihydroperylene (Pery_2H; see Figure 3) we will consider three structural isomers (Pery_2H_RamII, Pery_2H_RamIII, and Pery_2H_RamIV; see Figure 3). We will describe these isomers and their conformations in more detail below along with the structures of the other superhydrogenated perylenes.

To verify our computations, we compare our computational results with experimental measurements. Figure 5 shows the computed IR spectra (color lines) along with the experimental results (black line) for the hydrogenated species of naphthalene, i.e., Series A marked by Sandford et al. (2013).[5] In Figure 5, the red dashed lines represent the computational spectra applied with the frequency scale factor (γ) of ∼0.9688 given by Borowski (2012). As we can see, the scaled computational spectra are systematically blueshifted with respect to the experimental spectra. Hence, we determine an optimized scale factor of $\gamma \approx 0.963$. With this scale factor, the agreement between computations (purple solid lines) and experiments (black solid lines) is remarkably improved for bands, which correspond to pure fundamental vibrations, and this fact attests to the quality of our computations.

In Figure 6, we further compare our computational spectra of HHP (i.e., Pyre_6H, $C_{16}H_{16}$) and THB[a]p ($C_{20}H_{16}$; see Figure 4) with the experimental spectra of Sandford et al. (2013). As we can see, with a line width of 10 cm^{-1} and a scale factor of 0.963 for the frequencies, our calculations agree quite well with the experiments. Therefore, we believe that our calculations are reliable, and the optimized scaling factor of $\gamma = 0.963$ for frequencies will be applied in the following.

The intensity scaling is much more complicated than the frequency scaling, since the experimental data for the band intensities of hydrogenated PAHs are rare, and in band assignment it is often difficult to obtain a one-to-one correspondence between the experimental and computational spectra. Therefore, a common approach is to derive the relative strength, the strength of one band (e.g., the 3.4 μm band) relative to another band (e.g., the 3.3 μm band), and then compare the relative band strengths of the computational data with that of experimental data, with the band intensity obtained by integrating the intensity profile of the band, which contains several neighboring peaks. This will be discussed in detail in Section 3.4. In the following, we will present the calculated intensities without any scaling.

3. Results

3.1. Benzene Derivatives

We start from the smallest PAH molecule benzene and its hydrogenated derivatives. The computed total energies and thermochemical parameters are given in Table 1. The calculated

[5] We note that here the band strengths of the experimental spectra are scaled to that of the calculated spectra, since Sandford et al. (2013) did not report the absolute band strengths of these molecules.

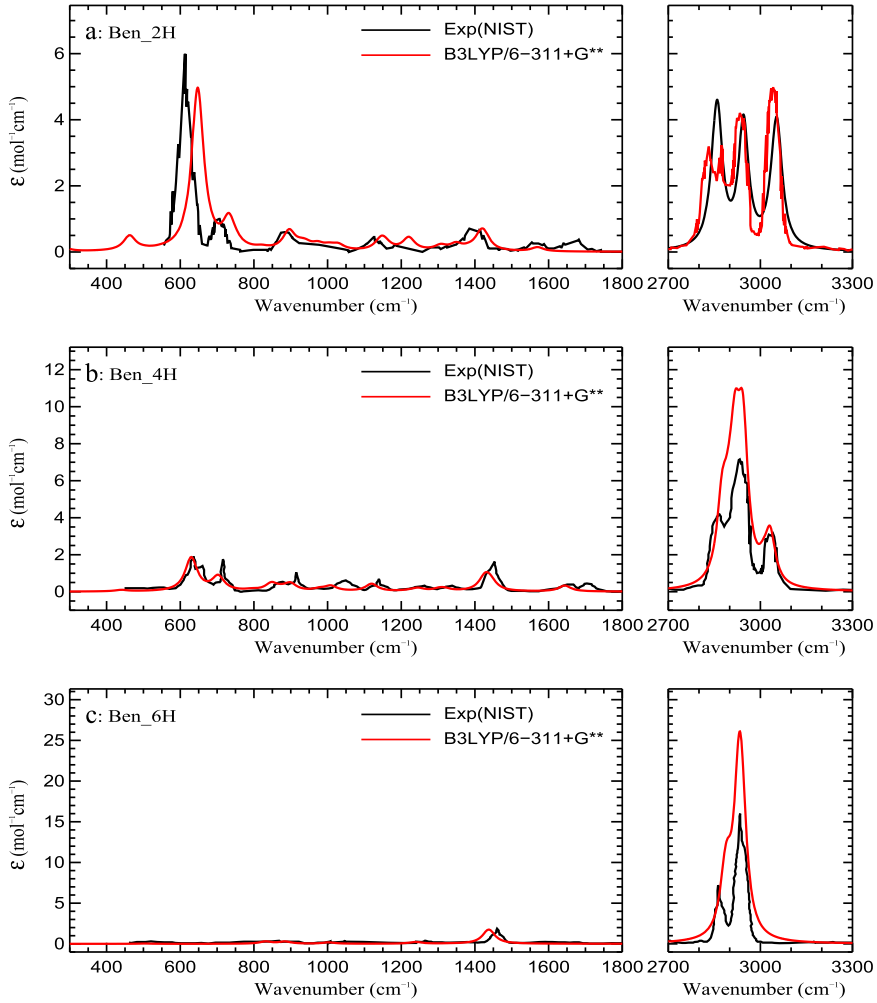

Figure 7. Comparison of the gas-phase absorption spectra experimentally measured by NIST (labeled with "Exp(NIST)"; red lines) with the computed, frequency-scaled spectra (black lines) of hydrogenated benzenes. The molar absorption coefficients ε for the NIST experimental data are scaled to be comparable to the computed spectra by multiplying the NIST absorbance with an artificial factor, as NIST only gives the absorbance and does not provide information on the concentration to derive ε.

spectra for neutral Ben_2H, Ben_4H, and Ben_6H are shown in Figure 7 along with the corresponding experimental spectra from the National Institute of Standards and Technology (NIST). The calculated frequencies are scaled with our optimized factor of $\gamma = 0.963$. For each spectral feature, we assign a line width of $20\,\mathrm{cm}^{-1}$. Since NIST only provides information about the absorbance but not the condensations, we cannot derive the absolute intensities for the features of the NIST experimental spectra. Therefore, we just scale the intensity of the NIST spectra with an appropriate factor to match our calculated spectra. Figure 7 shows that for Ben_2H, the calculation is in good agreement with the NIST experimental spectrum in the range of $\sim$2700–3300 cm^{-1}. In the range of $\sim$500–1500 cm^{-1}, a smaller scaling factor would lead to a better match. For Ben_4H and Ben_6H, the current scaling factor for frequencies already gives a satisfactory agreement with the experiment.

The upper panel of Figure 8 shows the spectra of neutral benzene, toluene (i.e., methyl-benzene), and all the hydrogenated species of benzene. It is quite clear that with the presence of aliphatic C–H bonds, the 3.4 μm feature (at $\sim$2900 cm^{-1}) arising from the aliphatic C–H stretch shows up.[6] Meanwhile, all the benzene derivatives except benzene also exhibit a feature at $\sim$450–500 cm^{-1}, which arises from the out-of-plane bending of aliphatic C–H. The aromatic C–C stretch at $\sim$6.8 μm (around 1470 cm^{-1}) of benzene becomes weaker in toluene, Ben_2H, and Ben_4H, and is absent in Ben_6H, in which all the C atoms are aliphatic.

The lower panel of Figure 8 shows the spectra of the cations of benzene and its hydrogenated derivatives as well as toluene. It is apparent that highly hydrogenated cations exhibit several strong features that are not seen in their neutral counterparts. For Ben_4H+, a feature at $\sim$1300 cm^{-1} originating from the aliphatic C–H out-of-plane bending is quite prominent. Ben_6H+ shows strong features at $\sim$380 cm^{-1} from the aliphatic C–C stretch, at $\sim$700 cm^{-1} from the aliphatic C–H out-of-plane bending, and at $\sim$840 cm^{-1} from the aliphatic C–H in-plane bending. Furthermore, the aliphatic C–H stretch features of cations occur at longer wavelengths with respect to the neutrals, especially for Ben_6H+. Moreover, all the C–H stretch features are significantly suppressed for cations, while their features in the range of $\sim$1200–1600 cm^{-1} are significantly enhanced.

The calculated intensities for the major aliphatic vibrational modes as well as the 3.3 and 6.2 μm aromatic modes are accumulated in Table 2. Unless otherwise noted, $A_{3.4}$, the band

[6] For benzene, all the C atoms are aromatic, while for Ben_6H, all the C atoms are aliphatic.

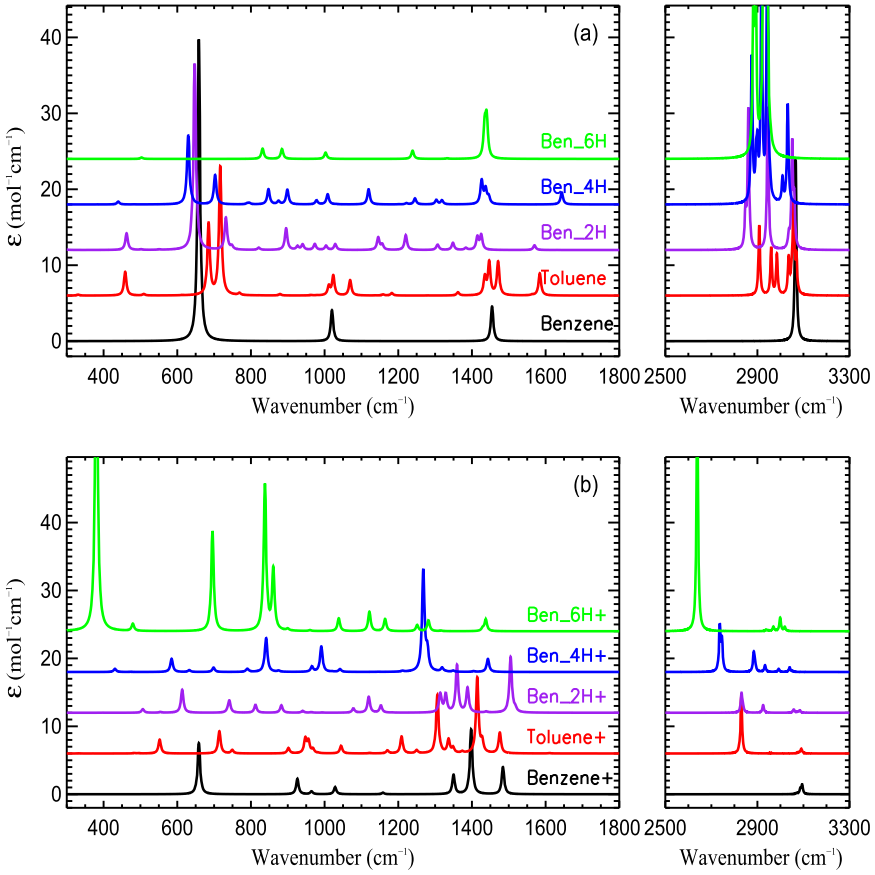

Figure 8. Comparison of the calculated spectra of hydrogenated benzenes with that of benzene and methyl-benzene (i.e., toluene). The upper panels are for neutrals and the lower ones are for cations. The frequencies are scaled with a factor of 0.963, and a line width of 4 cm^{-1} is assigned.

Table 2
IR Intensity (km mol^{-1}) of the 3.4 and 6.85 μm Aliphatic C–H Bands, the 3.3 μm Aromatic C–H Stretch Band, and the 6.2 μm Aromatic C–C Stretch Band Computed at the B3LYP/6−311+G** Level for All the Hydrogenated Benzenes as Shown in Figure 1

Compound	$A_{3.4}$	$A_{6.85}$	$A_{3.3}$	$A_{6.2}$	$A_{3.4}/A_{3.3}$	$A_{6.85}/A_{6.2}$
Ben_2H	32.92	0.49	16.54	0.49	1.99	1.00
Ben_4H	38.46	2.29	25.52	2.48	1.51	0.93
Ben_6H	45.39	2.33	…	…	…	…
Average	38.92	1.70	21.03	1.48	1.75	0.96
Ben_2H+	14.24	30.08	2.99	27.29	4.77	1.10
Ben_4H+	24.90	3.03	4.85	0.02	5.13	139.10
Ben_6H+	40.75	2.20	…	…	…	…
Average	26.63	11.77	3.92	13.65	4.95	70.10

Note. The $A_{3.3}$, $A_{3.4}$, and $A_{6.85}$ band strengths are on a per C–H bond basis, while the $A_{6.2}$ band strength is on a per C atom basis. Also tabulated are the band-strength ratios $A_{3.4}/A_{3.3}$ and $A_{6.85}/A_{6.2}$.

strength or intensity of the 3.4 μm aliphatic C–H stretch, and $A_{6.85}$, the band strength of the 6.85 μm aliphatic C–H deformation, are given on a per aliphatic C–H bond basis all through this paper. $A_{3.3}$, the band strength of the 3.3 μm aromatic C–H stretch, is given on a per aromatic C–H bond basis; and $A_{6.2}$, the band strength of the 6.2 μm C–C stretch, is given on a per aromatic C atom basis. The mean intensity for each feature obtained by averaging over all the hydrogenated derivatives of benzene (i.e., Ben_2H+, Ben_4H+, and Ben_6H+) is also tabulated in Table 2.

3.2. Naphthalene Derivatives

We then consider PAH molecules with two benzene rings, i.e., naphthalene and its hydrogenated derivatives. For this group, we calculate the vibrational spectra of five molecules (see Figure 2). The vibrational spectra of these molecules, marked as "Series A" in Sandford et al. (2013), were experimentally obtained by Sandford et al. (2013). This allows us to confront our computational spectra with the experimental spectra. The computed total energies and thermochemical parameters are given in Table 3.

The calculated spectra are shown in Figure 9, which clearly shows that for the aliphatic C–H stretch features, the neutrals have much higher intensities and peak at shorter wavelengths with respect to cations. For highly hydrogenated cations, e.g., Naph_10H, the aliphatic C–H stretch peaks at ∼3.5 μm. Meanwhile, the cations have much stronger features at ∼1300–1500 cm^{-1} than the neutrals, just like the benzene derivatives. For methylated naphthalene, as shown in Figure 9, the aliphatic C–H stretch also shows up in the computed spectra, but not as pronounced as hydrogenated naphthalene. Also, compared with hydrogenated naphthalene, the aliphatic C–H stretch of methylated naphthalene occurs at somewhat shorter wavelengths.

The intensities of the major aliphatic vibrational modes for the hydrogenated cations are shown in Table 4. Also tabulated are the mean intensities of individual features obtained by averaging over all five hydrogenated cations. For c-PHN (i.e., Naph_10Ha; see Figure 2) and t-PHN (i.e., Naph_10Hb; see Figure 2), they are fully hydrogenated and thus have no

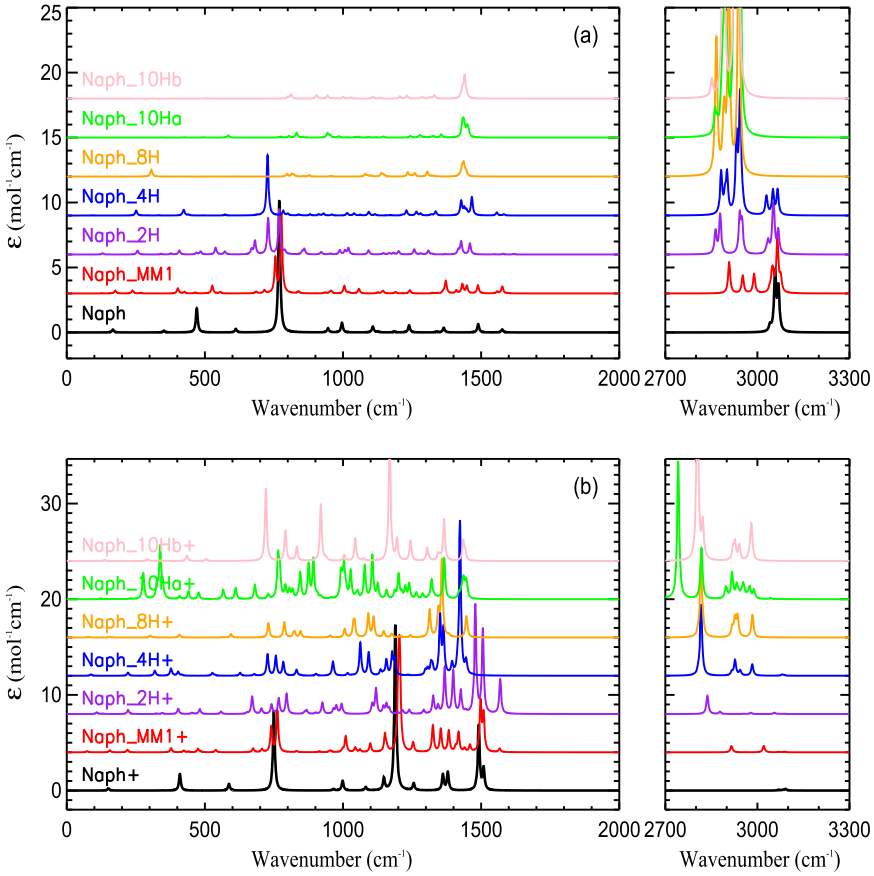

Figure 9. Same as Figure 8 but for naphthalene and its hydrogenated and mono-methylated derivatives, where "MM1" refers to mono-methylated species in which the methyl group is attached at position "1" of a PAH molecule according to standard International Union of Pure and Applied Chemistry (IUPAC) numbering.

aromatic features.[7] They are both fully hydrogenated and thus have no aromatic features. For OHN (i.e., Naph_8H; see Figure 2), although it is not fully hydrogenated, it has no H attached to aromatic C atoms and thus the 3.3 μm aromatic C–H stretch is also absent. The aromatic C–C stretch features are seriously suppressed and essentially have negligible intensities for both neutrals and cations.

3.3. Perylene Derivatives

A larger PAH molecule, perylene ($C_{20}H_{12}$), which has as many edge C atoms as possible to be hydrogenated for PAHs of five six-membered rings, is selected as our next sample. A series of extra H atoms has been considered, from two all the way up to 14, which corresponds to a complete hydrogenation of all the edge C atoms. For each situation, we consider several isomers of which the extra H atoms are attached at different positions. Table 5 presents the computed total energies and thermochemical parameters for the neutrals and cations, respectively.

We show in Figures 10–15 the calculated spectra for each hydrogenation along with that of perylene and methyl-perylene.[8] In all these figures, the neutrals are displayed in the upper panels, and the cations appear in the lower ones. For the neutrals, the spectra do not seem to exhibit significant differences among different isomers. Again, the most prominent aliphatic feature is the aliphatic C–H stretch at 3.4 μm for all the neutrals that become stronger with the degree of hydrogenation and show a strong peak around 2950 cm^{-1} accompanied by a series of satellite features at longer wavelengths. As the number of extra H atoms increases, the aromatic features become weaker as expected and tend to shift to the red side, especially for heavy hydrogenations (e.g., superhydrogenated perylene with eight or more extra H atoms). On the other hand, the aliphatic C–H deformation bands at 6.85 μm (1470 cm^{-1}) and 7.45 μm (1310 cm^{-1}) become stronger as the hydrogenation increases. Moreover, the aliphatic C–H stretch of methyl-perylene appears to occur at a shorter wavelength than perylene. Compared with that of the neutral molecules, both the 3.3 μm aromatic and 3.4 μm aliphatic C–H stretch features are significantly suppressed for all the cations, while the cationic C–C stretch and C–H bending bands at ~1200–1600 cm^{-1} are considerably enhanced. This is similar to benzene and naphthalene and their derivatives. Unfortunately, we cannot compare these computed spectra with the experimental spectra, since to our knowledge, there are no experimental data available for the perylene derivatives.

The intensities computed for the aliphatic bands at 3.4 and 6.85 μm and the aromatic bands at 3.3 and 6.2 μm are shown in Table 6. Also tabulated in Tables 6 are the mean intensities for each band, obtained by averaging over all the derivatives of perylene.

[7] The fully hydrogenated species c-PHN and t-PHN are isomers. For c-PHN, the hydrogen atoms attached to the two carbon atoms at the junction of the two benzene rings are on the same side of the PAH plane, while for t-PHN the hydrogen atoms are on the opposite side.

[8] For Pery_14H, only one isomer is calculated, so its spectrum is shown with the Pery_12H isomers in Figure 10–15.

Table 3
Same as Table 1 but for the Hydrogenated Derivatives of Naphthalene as Shown in Figure 2

Compound	E_{tot}	VZPE	TE	S	ν_1	ν_2	μ
DHN (Naph_2H)	−387.180337	106.21	110.92	85.00	134.45	152.34	0.6693
THN (Naph_4H)	−388.405052	121.04	126.01	85.70	96.16	143.04	0.7829
OHN (Naph_8H)	−390.810255	149.73	155.35	88.65	91.21	141.58	0.0000
c-PHN (Naph_10Ha)	−392.031003	165.09	170.64	88.69	138.52	154.01	0.0269
t-PHN (Naph_10Hb)	−392.036103	164.83	170.42	89.19	128.35	138.68	0.0000
DHN+	−386.898228	105.83	110.70	87.72	113.20	135.78	1.1938
THN+	−388.101882	119.58	124.85	89.52	88.20	91.18	2.0163
OHN+	−390.524810	148.44	154.25	91.85	81.26	81.49	0.0000
c-PHN+	−391.691884	160.73	166.81	94.67	126.77	141.78	2.2291
t-PHN+	−391.706269	161.77	167.83	93.38	109.62	143.02	0.0000

Table 4
Same as Table 2 but for the Hydrogenated Derivatives of Naphthalene as Shown in Figure 2

Compound	$A_{3.4}$	$A_{6.85}$	$A_{3.3}$	$A_{6.2}$	$A_{3.4}/A_{3.3}$	$A_{6.85}/A_{6.2}$
DHN (Naph_2H)	31.05	4.16	15.28	0.17	2.03	24.85
THN (Naph_4H)	35.85	3.00	16.43	0.68	2.18	4.40
OHN (Naph_8H)	44.40	1.61	…	0.00	…	…
c-PHN (Naph_10Ha)	44.65	2.29	…	…	…	…
t-PHN (Naph_10Hb)	43.61	1.91	…	…	…	…
Average	39.91	2.59	15.85	0.28	2.11	14.62
DHN+	7.28	28.67	0.39	37.49	18.82	0.76
THN+	17.87	2.32	0.59	0.12	30.28	19.69
OHN+	12.61	1.91	…	0.00	…	…
c-PHN+	28.65	4.08	…	…	…	…
t-PHN+	21.81	1.99	…	…	…	…
Average	17.64	7.79	0.49	12.54	24.55	10.23

3.4. The Sandford et al. (2013) Molecules

Sandford et al. (2013) obtained the 2.5–20 μm (i.e., 500–4000 cm^{-1}) absorption spectra of 23 hydrogenated PAHs and related molecules isolated in the argon matrix at 15 K. We now consider all the hydrogenated PAH species experimentally studied by Sandford et al. (2013) except the derivatives of naphthalene, i.e., Series B to Series H as marked by Sandford et al. (2013), which have already been discussed in detail in Section 3.2. To highlight the vibrational features originated from the addition of extra H atoms, we also calculate the vibrational spectra of the parental molecules, e.g., the parental molecule of the Series B molecules of Sandford et al. (2013) is anthracene ($C_{14}H_{10}$). Again, we consider both neutrals and cations and tabulate in Table 7 the computed total energies and thermochemical parameters for these molecules.

In Figures 16–22 we present the calculated spectra, with each figure for one group of which the molecules share the same parent (e.g., Figure 11 is for the derivatives of anthracene, and Figure 12 is for the derivatives of phenanthrene). Again, we also show in each figure the spectra computed for the mono-methylated molecules. It is apparent that, as shown in the upper panel of each figure, all hydrogenated neutral molecules exhibit the aliphatic C–H stretching feature around 3.4 μm. This feature is also seen in methylated neutral molecules but at a slightly shorter wavelength. The aliphatic C–H deformation feature at ∼6.85 μm is also prominent in the spectra of all the molecules in the range of ∼1400–1450 cm^{-1}. However, the 7.25 μm aliphatic C–H deformation feature at ∼1350–1400 cm^{-1} is much less pronounced. In Table 8 we present the intensities of the 3.4 and 6.85 μm aliphatic C–H bands as well as the 3.3 and 6.2 μm aromatic bands. Also tabulated are the corresponding aliphatic-to-aromatic intensity ratios $A_{3.4}/A_{3.3}$ and $A_{6.85}/A_{6.2}$. Similarly, we show in the lower panel of each figure the spectra of the cationic counterparts of those presented in the upper panel. Clearly, the C–H stretch at ∼3.4 μm is considerably reduced while the C–C stretching and C–H bending features in ∼1200–1600 cm^{-1} are remarkably enhanced. The intensities of the 3.3, 3.4, 6.2, and 6.85 μm bands calculated for the cationic species are also tabulated in Table 8. For both neutrals and cations, we also derive the mean intensity for each band by averaging over all the derivatives (see Table 8).

In Figure 23 we show $A_{CH,ali}/A_{CH,aro}$ as a function of $N_{H,ali}/N_{H,aro}$, where $A_{CH,ali}$ is the intensity of the 3.4 μm aliphatic C–H stretch of a given molecule, $A_{CH,aro}$ is the intensity of the 3.3 μm aromatic C–H stretch of the given molecule, and $N_{H,ali}$ and $N_{H,aro}$ are respectively the total number of aliphatic and aromatic C–H bonds of the given molecule. The slope of the line fit to the data in Figure 23 is $d(A_{CH,ali}/A_{CH,aro})/d(N_{H,ali}/N_{H,aro}) \approx 1.85$, which is lower than that of Sandford et al. (2013) by ∼33%. This difference appears to be mainly caused by heavily hydrogenated species HHP (Pyre_6H, $C_{16}H_{16}$) and THB[a]P ($C_{20}H_{16}$), and slightly hydrogenated species 9H-Cp[a]P ($C_{19}H_{12}$) and 11HB[b]F ($C_{17}H_{12}$). The difference would be reduced to within 10% if these species are excluded. Compared with the spectra of Sandford et al. (2013) obtained from the matrix isolation spectroscopy, the $A_{CH,ali}/A_{CH,aro}$ intensity ratios computed here for HHP and THB[a]P are appreciably lower. As illustrated in Figure 6, the computed spectra for both molecules are in close agreement with the experimental spectra of Sandford et al. (2013), except the experimental spectra exhibit an extra feature at ∼2840 cm^{-1}. This

Table 5
Same as Table 1 but for the Hydrogenated Derivatives of Perylene as Shown in Figure 3

Compound	E_{tot}	VZPE	TE	S	ν_1	ν_2	μ
Pery_2H_RamII	−770.753921	172.62	181.11	114.95	37.33	64.53	0.6515
Pery_2H_RamIII	−770.772978	172.78	181.24	113.61	50.92	92.01	0.8480
Pery_2H_RamIV	−770.744407	172.18	180.77	114.57	49.57	84.50	0.7150
Pery_4H	−771.953401	187.06	195.83	115.86	47.24	86.27	1.0315
Pery_4H_RG1	−771.951377	186.87	195.70	116.69	34.57	85.78	1.3194
Pery_4H_RG2	−771.986296	187.76	196.38	114.93	51.61	77.12	0.9694
Pery_6H	−773.178734	201.90	210.92	117.59	40.81	84.47	1.3198
Pery_6H_Yal	−773.205900	202.12	211.18	118.20	50.54	60.42	1.4594
Pery_6H1_Yal	−773.205072	202.04	211.17	119.50	42.50	52.96	1.4314
Pery_6H_ZinkeR	−773.196404	202.07	211.12	117.66	57.26	73.40	0.0460
Pery_6H1_Zinke	−773.196165	202.09	211.15	117.85	56.58	67.78	0.0000
Pery_8H	−774.333885	215.26	224.77	120.87	39.69	78.16	1.4590
Pery_8Hb	−774.335840	215.32	224.79	119.99	53.13	81.01	1.4564
Pery_8H_Yal	−774.404986	216.86	226.01	118.14	62.98	69.23	1.3854
Pery_8Hb_Yal	−774.392233	216.94	226.17	119.13	52.82	80.29	1.4419
Pery_8H_Zinke	−774.398164	216.87	225.97	117.79	57.52	76.52	0.5307
Pery_8Hb_Zinke	−774.385387	216.62	226.01	123.33	15.58	56.86	0.0000
Pery_8H_RG1	−774.384872	216.71	225.97	119.82	28.89	86.27	1.4488
Pery_8H_RG2	−774.387559	216.72	225.82	117.94	38.78	84.51	1.1210
Pery_10H	−775.541432	230.08	239.83	122.70	42.09	73.37	0.9738
Pery_10Hb	−775.539497	230.09	239.77	121.83	45.13	78.15	1.0945
Pery_10H_RG1	−775.612714	231.25	240.85	121.84	49.44	62.02	1.0798
Pery_10H_RG2	−775.563323	231.13	240.68	121.99	31.45	68.40	1.3365
Pery_12H	−776.766232	244.94	254.92	124.01	43.15	71.18	0.3473
Pery_12Hb	−776.768985	245.00	254.95	123.31	51.44	78.04	0.2981
Pery_12H_RG1	−776.800583	245.45	255.36	123.69	48.54	67.71	0.5676
Pery_12H_RG2	−776.799299	245.29	255.38	125.67	45.82	64.18	0.5083
Pery_14H_Yal	−778.023443	260.28	270.43	125.47	45.81	69.16	0.0643
HC_Pery_2H_RamII+	−770.496974	172.38	180.96	116.38	43.61	76.94	2.1098
HC_Pery_2H_RamIII+	−770.526761	172.81	181.40	116.28	44.18	85.96	1.4860
HC_Pery_2H_RamIV+	−770.522678	172.73	181.35	116.50	45.79	79.38	1.3025
HC_Pery_4H+	−771.723440	187.41	196.25	117.96	44.23	80.46	0.9571
HC_Pery_4H_RG1+	−771.716524	187.11	196.01	118.63	36.45	81.25	0.7951
HC_Pery_4H_RG2+	−771.728963	187.68	196.49	118.58	33.29	66.61	2.1650
HC_Pery_6H+	−772.940502	202.02	211.15	120.29	32.91	77.56	1.6254
HC_Pery_6H_Yal+	−772.951020	201.91	211.10	119.31	42.03	65.22	0.2005
HC_Pery_6H1_Yal+	−772.949412	201.75	211.09	124.84	13.04	56.54	0.3613
HC_Pery_6H_ZinkeR+	−772.956553	202.26	211.42	120.29	52.95	64.70	0.3530
HC_Pery_6H1_Zinke+	−772.956228	202.28	211.45	120.67	49.67	58.93	0.0000
HC_Pery_8H+	−774.122849	215.74	225.31	123.40	31.23	71.19	1.8918
HC_Pery_8Hb+	−774.123811	215.78	225.32	122.39	44.13	75.32	1.8700
HC_Pery_8H_Yal+	−774.136447	216.67	226.01	121.08	59.84	61.18	2.2739
HC_Pery_8Hb_Yal+	−774.125730	216.70	226.11	121.97	50.31	72.40	1.8594
HC_Pery_8H_Zinke+	−774.110956	214.71	224.21	122.23	47.63	68.01	0.8075
HC_Pery_8Hb_Zinke+	−774.105278	214.94	224.50	123.41	40.66	65.24	1.1675
HC_Pery_8H_RG1+	−774.144315	216.82	226.08	120.61	47.50	73.98	2.0791
HC_Pery_8H_RG2+	−774.131549	216.60	225.84	120.41	37.24	79.73	3.6216
HC_Pery_10H+	−775.323173	230.35	240.17	125.04	35.95	71.65	2.4960
HC_Pery_10Hb+	−775.322751	230.44	240.36	126.68	29.92	62.85	2.4753
HC_Pery_10H_RG1+	−775.359377	230.97	240.76	125.13	39.86	60.39	2.3740
HC_Pery_10H_RG2+	−775.325197	231.10	240.59	121.93	53.18	65.83	3.4206
HC_Pery_12H+	−776.541119	245.01	255.12	127.38	28.86	67.25	2.3983
HC_Pery_12Hb+	−776.542472	245.10	255.15	126.20	36.41	72.09	2.4220
HC_Pery_12H_RG1+	−776.544666	245.15	255.25	127.08	38.21	63.75	2.8541
HC_Pery_12H_RG2+	−776.549805	244.92	255.13	128.35	42.55	49.79	3.7425
HC_Pery_14H_Yal+	−777.754163	258.90	269.47	131.13	28.64	63.37	0.0418

would raise $A_{CH,ali}$ and therefore result in a larger slope for the experimental data. Moreover, Pauzat & Ellinger (2001) performed DFT calculations on hydrogenated naphthalene, anthracene, and pyrene and obtained $d(A_{CH,ali}/A_{CH,aro})/d(N_{H,ali}/N_{H,aro}) \approx 1.74$, which is close to the value derived here.

Maltseva et al. (2018) applied advanced laser spectroscopic techniques combined with mass spectrometry to obtain the gas-phase absorption spectra of four supersonically cooled super-hydrogenated PAH species in the 3.175–3.636 μm wavelength region, including slightly hydrogenated DHA and DHPh

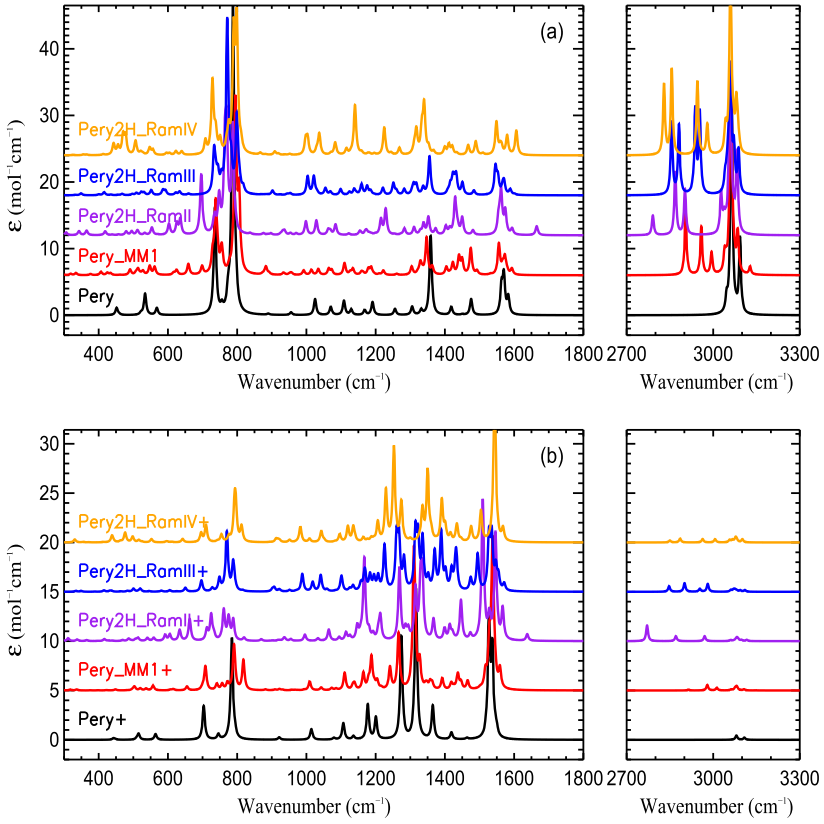

Figure 10. Comparison of the calculated spectra of Pery_2H (perylene with two excess H atoms) with that of perylene and methyl-perylene. The upper panels are for neutrals and the lower ones are for cations. The frequencies are scaled with a factor of 0.963, and a line width of 4 cm^{-1} is assigned.

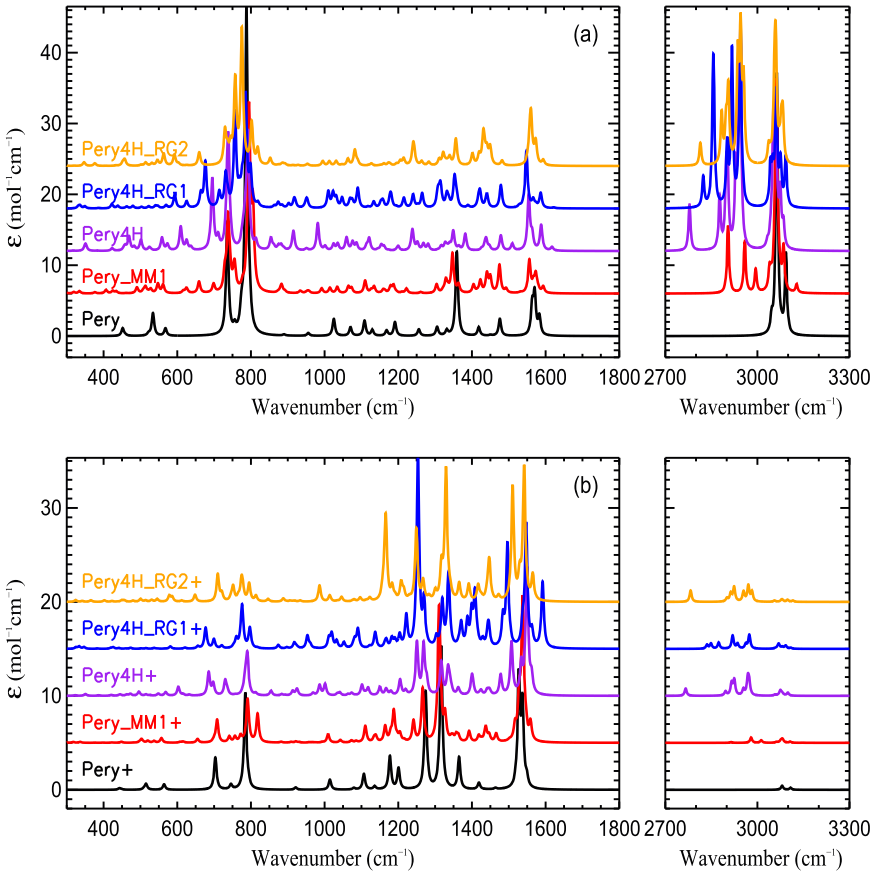

Figure 11. Continued, but for Pery_4H (perylene with four excess H atoms).

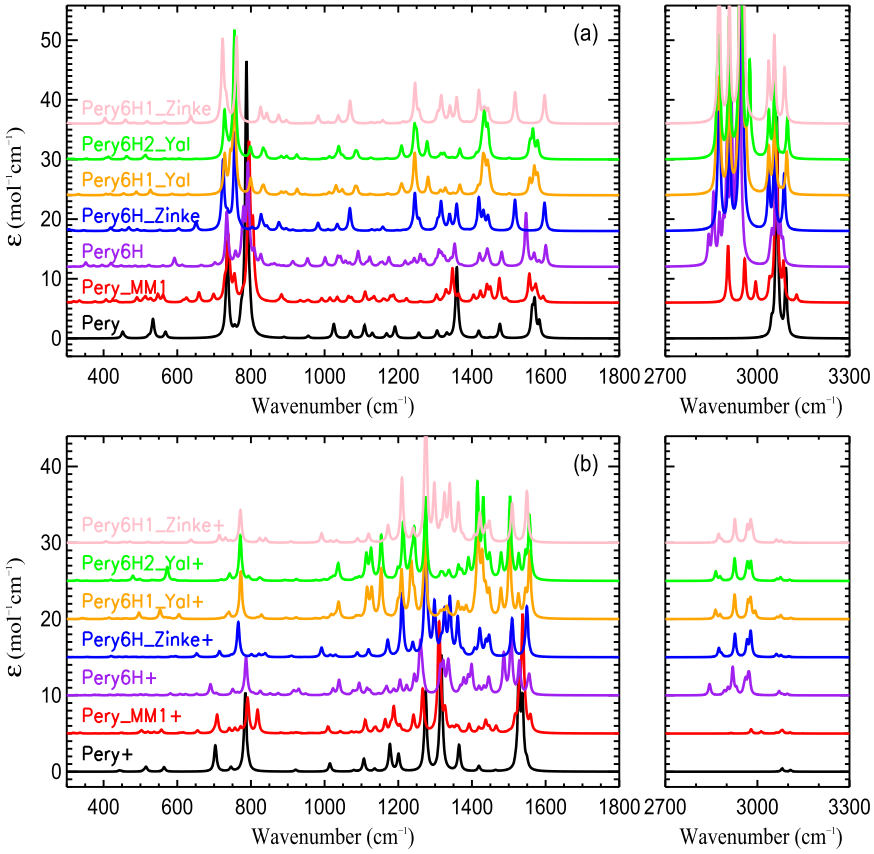

Figure 12. Continued, but for Pery_6H (perylene with six excess H atoms).

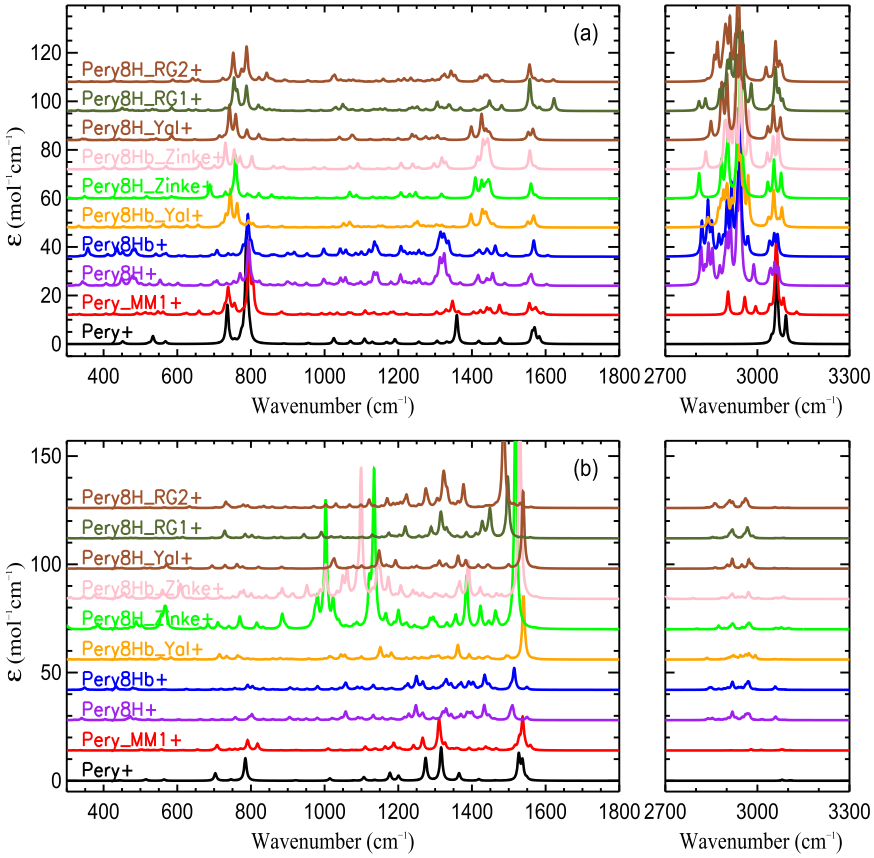

Figure 13. Continued, but for Pery_8H (perylene with eight excess H atoms).

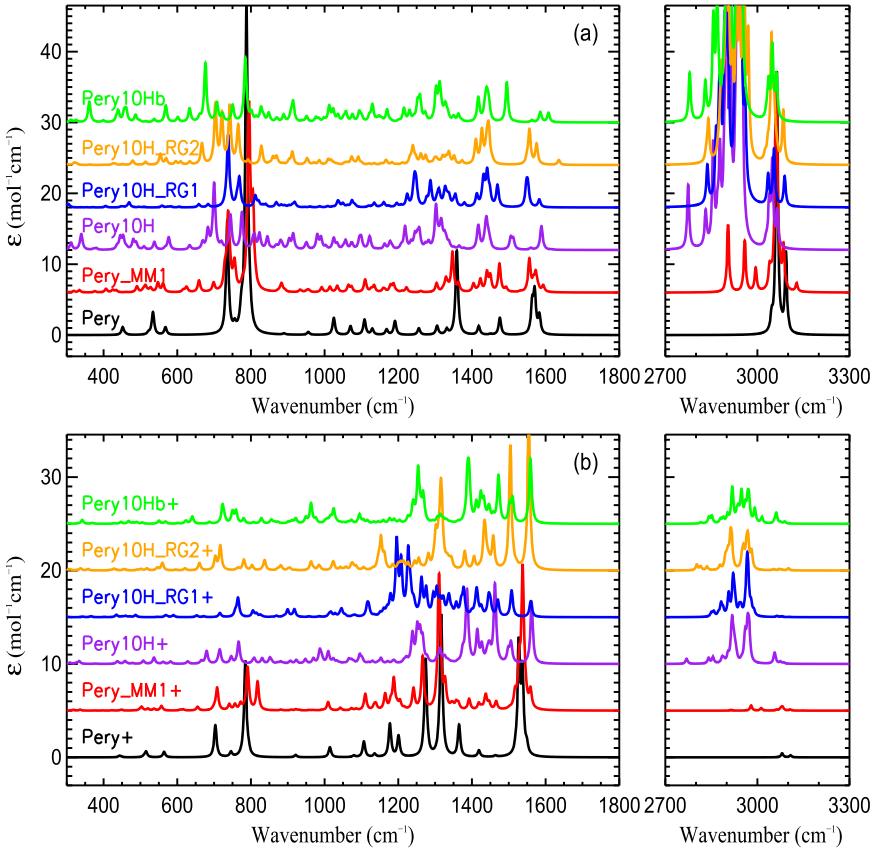

Figure 14. Continued, but for Pery_10H (perylene with ten excess H atoms).

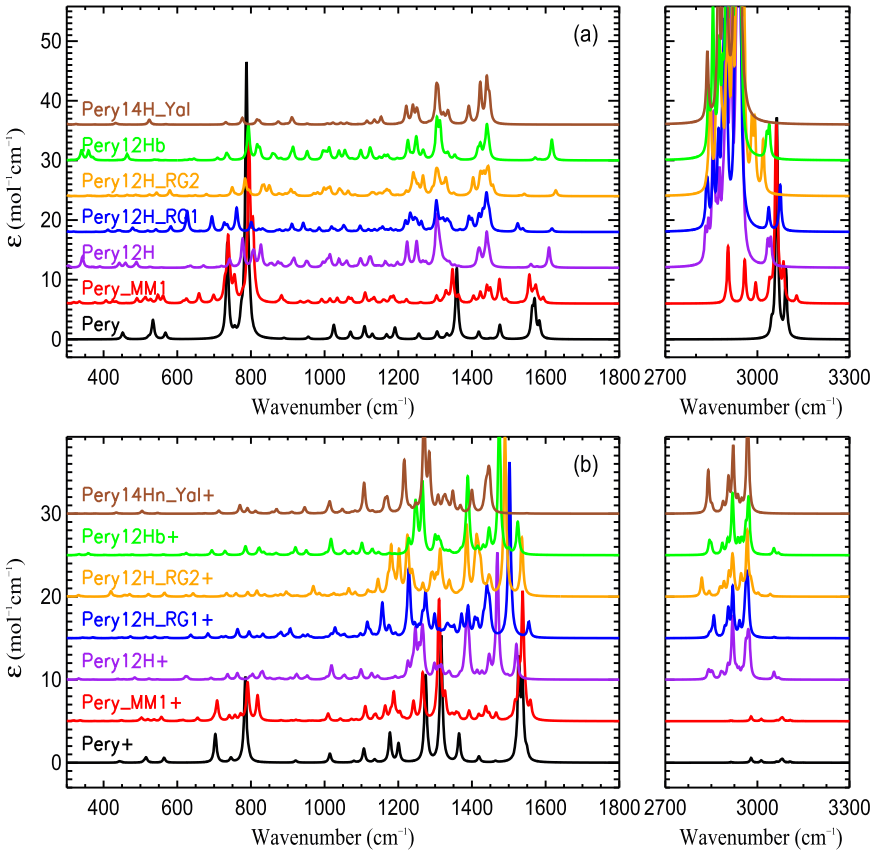

Figure 15. Continued, but for Pery_12H (perylene with 12 excess H atoms) and Pery_14H (perylene with 14 excess H atoms).

Table 6
Same as Table 2 but for the Hydrogenated Derivatives of Perylene as Shown in Figure 3

Compound	$A_{3.4}$	$A_{6.85}$	$A_{3.3}$	$A_{6.2}$	$A_{3.4}/A_{3.3}$	$A_{6.85}/A_{6.2}$
Pery_2H_RamII	20.13	4.83	14.61	2.65	1.38	1.82
Pery_2H_RamIII	36.05	3.54	12.95	1.76	2.78	2.01
Pery_2H_RamIV	30.63	1.35	14.54	2.70	2.11	0.50
Pery_4H	34.47	0.87	16.06	2.89	2.15	0.30
Pery_4H_RG1	38.10	1.47	13.65	2.33	2.79	0.63
Pery_4H_RG2	30.53	2.96	14.10	2.73	2.17	1.09
Pery_6H	39.43	1.59	14.02	3.94	2.81	0.40
Pery_6H_Yal	34.57	2.02	15.67	2.17	2.21	0.93
Pery_6H1_Yal	34.86	2.92	15.63	2.20	2.23	1.32
Pery_6H_ZinkeR	33.73	3.20	17.30	2.75	1.95	1.16
Pery_6H1_Zinke	33.82	2.72	17.33	2.24	1.95	1.21
Pery_8H	41.49	1.72	16.19	3.48	2.56	0.50
Pery_8Hb	40.25	1.54	14.58	3.41	2.76	0.45
Pery_8H_Yal	33.95	2.96	15.33	1.98	2.21	1.49
Pery_8Hb_Yal	34.12	1.48	15.18	2.26	2.25	0.66
Pery_8H_Zinke	32.59	3.81	16.35	1.85	1.99	2.06
Pery_8Hb_Zinke	27.87	6.15	25.54	2.22	1.09	2.77
Pery_8H_RG1	35.75	1.28	15.65	5.95	2.28	0.22
Pery_8H_RG2	36.46	1.38	14.85	2.77	2.45	0.50
Pery_10H	40.28	1.59	18.30	2.07	2.20	0.77
Pery_10Hb	39.28	1.74	17.16	2.48	2.29	0.70
Pery_10H_RG1	38.74	1.92	21.21	1.99	1.83	0.97
Pery_10H_RG2	32.73	2.19	18.97	2.82	1.73	0.78
Pery_12H	42.09	1.56	12.97	1.62	3.24	0.96
Pery_12Hb	42.14	1.49	13.47	1.58	3.13	0.95
Pery_12H_RG1	39.62	1.84	17.91	0.96	2.21	1.91
Pery_12H_RG2	39.01	1.81	30.13	0.55	1.29	3.29
Average	35.66	2.29	16.65	2.46	2.22	1.12
Pery_2H_RamII+	10.83	9.99	1.04	21.98	10.45	0.45
Pery_2H_RamIII+	7.94	38.26	1.23	13.72	6.46	2.79
Pery_2H_RamIV+	3.96	19.57	1.82	15.18	2.17	1.29
Pery_4H+	13.85	5.04	1.77	20.77	7.82	0.24
Pery_4H_RG1+	9.80	14.52	1.78	29.49	5.51	0.49
Pery_4H_RG2+	13.78	11.54	1.13	24.94	12.16	0.46
Pery_6H+	15.15	8.85	1.63	16.42	9.32	0.54
Pery_6H2_Yal+	10.07	11.91	1.86	22.29	5.42	0.53
Pery_6H1_Yal+	10.85	28.83	1.90	25.93	5.71	1.11
Pery_6H_Zinke+	10.39	13.39	1.63	12.07	6.37	1.11
Pery_6H1_Zinke+	10.55	6.96	1.65	12.74	6.40	0.55
Pery_8H+	13.54	7.78	5.09	13.24	2.66	0.59
Pery_8Hb+	12.97	12.90	4.60	13.53	2.82	0.95
Pery_8H_Yal+	13.02	2.93	1.04	39.28	12.57	0.07
Pery_8Hb_Yal+	13.02	2.66	0.95	33.44	13.65	0.08
Pery_8H_Zinke+	13.37	9.34	4.70	117.20	2.85	0.08
Pery_8Hb_Zinke+	10.67	19.65	4.90	103.34	2.18	0.19
Pery_8H_RG1+	14.52	19.37	0.75	30.54	19.39	0.63
Pery_8H_RG2+	18.17	50.40	1.25	2.32	14.55	21.71
Pery_10H+	14.75	2.73	4.93	22.99	2.99	0.12
Pery_10Hb+	14.14	8.50	5.18	18.49	2.73	0.46
Pery_10H_RG1+	15.32	7.00	2.20	7.70	6.96	0.91
Pery_10H_RG2+	15.79	4.48	1.20	42.06	13.14	0.11
Pery_12H+	14.76	7.58	6.86	30.68	2.15	0.25
Pery_12Hb+	14.85	7.70	6.53	33.82	2.28	0.23
Pery_12H_RG1+	15.78	9.57	0.82	36.09	19.24	0.27

Table 6
(Continued)

Compound	$A_{3.4}$	$A_{6.85}$	$A_{3.3}$	$A_{6.2}$	$A_{3.4}/A_{3.3}$	$A_{6.85}/A_{6.2}$
Pery_12H_RG2+	14.99	12.95	3.69	41.99	4.07	0.31
Average	12.85	13.13	2.67	29.71	7.48	1.35

Table 7
Same as Table 1 but for the Sandford et al. (2013) Molecules as Shown in Figure 4 at the B3LYP/6-311+G** Level

Compound	E_{tot}	VZPE	TE	S	ν_1	ν_2	μ
DHA	−540.868165	135.60	141.90	96.93	53.31	122.15	0.3557
HHA	−543.219349	162.56	170.10	108.79	36.87	70.27	0.0023
DHPh	−540.871768	135.93	142.18	96.05	86.59	103.76	0.5922
DBS	−580.183622	153.93	160.91	103.72	42.47	93.64	0.5200
tPHF	−508.771366	205.07	212.43	105.17	60.46	104.25	0.0993
DHP	−617.117922	143.84	150.51	98.63	86.75	134.11	0.6216
HHP	−619.530713	172.79	180.11	104.72	84.13	97.29	0.0000
THBaP	−772.007230	187.51	196.24	115.50	54.77	78.13	1.1531
H9CpaP	−731.455224	154.18	161.96	108.25	67.45	113.41	0.8871
HHCpaP	−731.455224	154.18	161.96	108.25	67.45	113.41	0.8871
DDHTP	−700.577894	237.65	247.33	123.09	50.06	76.72	0.0340
PHC	−936.545478	349.56	361.11	132.27	64.00	64.14	0.0000
DHBdeA	−656.439215	161.77	169.27	106.81	67.38	85.13	0.9977
CpPh	−577.776337	125.39	131.42	95.40	94.07	184.13	0.6588
HBbF	−655.222412	146.60	153.90	105.83	60.67	95.01	0.6798
DHDBahA	−848.218890	194.02	203.80	126.06	19.21	48.09	0.0000
DHBep	−770.778358	172.70	181.23	114.08	61.35	81.20	0.7271
TRIP	−770.756412	172.81	181.11	113.02	66.45	66.53	0.0001
DHA+	−540.572936	133.52	140.23	102.32	28.03	93.78	0.2662
HHA+	−542.936608	160.22	167.84	109.54	52.80	83.74	0.1517
DHPh+	−540.593203	135.71	142.15	99.01	72.67	95.49	0.1409
DBS+	−579.894009	153.31	160.50	107.12	34.65	80.78	0.3793
tPHF+	−508.448630	202.54	210.39	109.82	53.47	95.12	3.2675
DHP+	−616.844866	143.39	150.23	101.20	83.70	124.12	0.8562
HHP+	−619.272752	172.53	180.02	107.46	81.67	85.99	0.0000
THBaP+	−771.755072	187.51	196.35	117.79	54.83	69.96	2.1796
H9CpaP+	−731.199725	154.07	161.94	110.34	68.24	105.24	1.2416
HHCpaP+	−734.823483	197.89	206.82	118.72	45.45	81.58	0.6217
DDHTP+	−700.312268	236.08	246.05	124.76	52.59	67.68	0.1916
PHC+	−936.252216	346.64	358.57	135.86	61.64	64.77	0.0000
DHBdeA+	−656.173080	161.47	169.14	109.63	58.14	80.12	0.5296
CpPh+	−577.500270	124.81	130.97	97.57	96.68	175.49	0.1925
HBbF+	−654.956057	146.56	153.97	108.03	57.63	93.88	0.8366
DHDBahA+	−847.951115	193.15	203.14	130.79	8.46	41.40	0.0000
DHBep+	−770.529159	172.76	181.39	116.62	56.46	66.49	0.9530
TRIP+	−770.480563	172.58	181.08	116.10	63.07	63.16	0.0000

(see Figure 4) and heavily hydrogenated THN (see Figure 2) and HHP (see Figure 4). They obtained a slope of $d(A_{CH,ali}/A_{CH,aro})/d(N_{H,ali}/N_{H,aro}) \approx 1.57$, which is closer to that derived here but considerably lower than that of Sandford et al. (2013).[9] Maltseva et al. (2018) argued that the difference might be traced back to the influence of the environment on band intensities. It is known that the incorporation of PAHs into rare gas matrices could cause a suppression on the intensities of the vibrational bands compared to that of isolated molecules (Joblin et al. 1994). Maltseva et al. (2018) speculated that it is possible that aromatic C–H stretch bands might be suppressed to a larger extent under rare gas matrix conditions than aliphatic C–H stretch bands. However, as shown in Figure 6, the relative strengths of the aliphatic and aromatic C–H stretches of HHP and THB[a]P of Sandford et al. (2013) measured with the matrix isolation spectroscopy method agree closely with that computed here, except that the experimental spectra show an extra feature at $\sim$2840 cm^{-1} that is not seen in the computed spectra.

In future work, a more precise assignment of the experimental and computational spectral bands of hydrogenated PAHs and accurate intensity scaling would be necessary for accurately determining their band strengths. Based on what

[9] Maltseva et al. (2018) also obtained the experimental spectra of methylated PAHs in the C–H stretch wavelength region. The aliphatic-to-aromatic C–H stretch band ratio of methylated PAHs experimentally derived by Maltseva et al. (2018) is close to that determined from quantum-chemical computations (see Yang et al. 2013, 2016b).

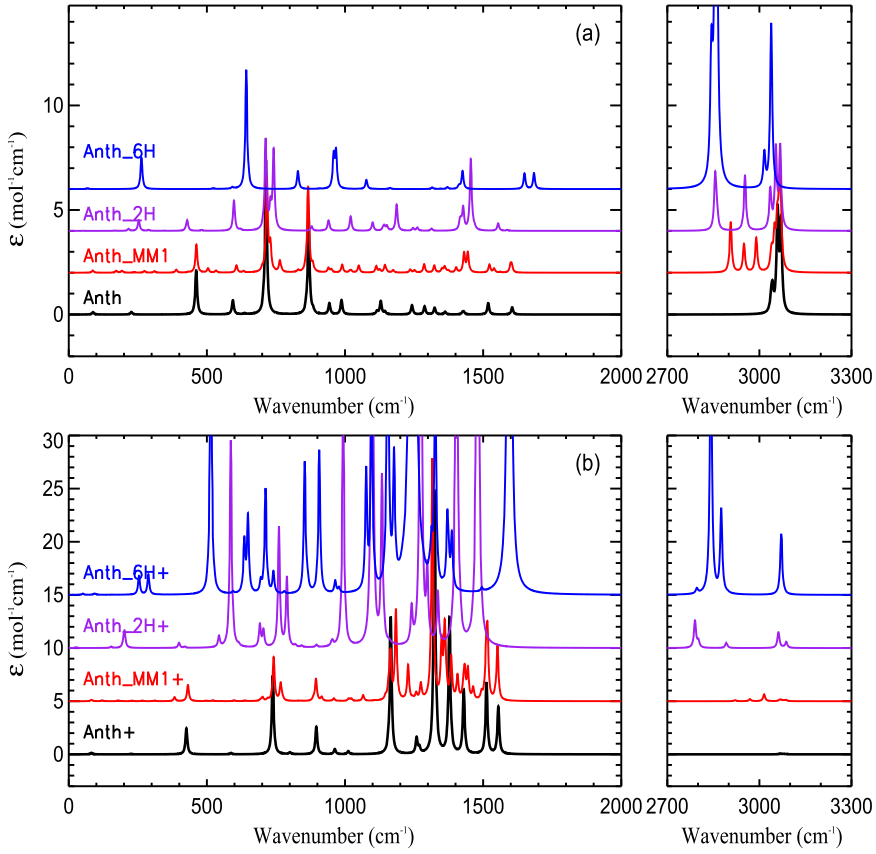

Figure 16. Calculated vibrational spectra of neutral (upper panels) and cationic (lower panels) anthracene derivatives ("Series B" of Sandford et al. 2013) compared with anthracene and mono-methylated-anthracene. The frequencies are scaled with a factor of 0.963, and a line width of 4 cm^{-1} is assigned.

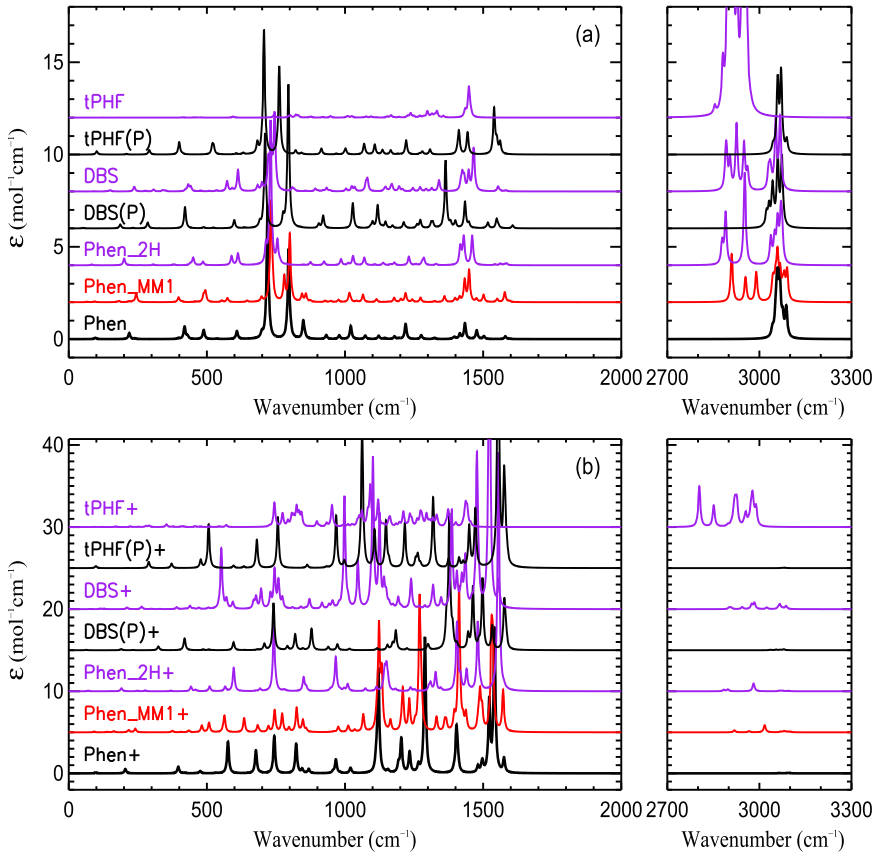

Figure 17. Continued, but for the derivatives of phenanthrene ("Series C" of Sandford et al. 2013).

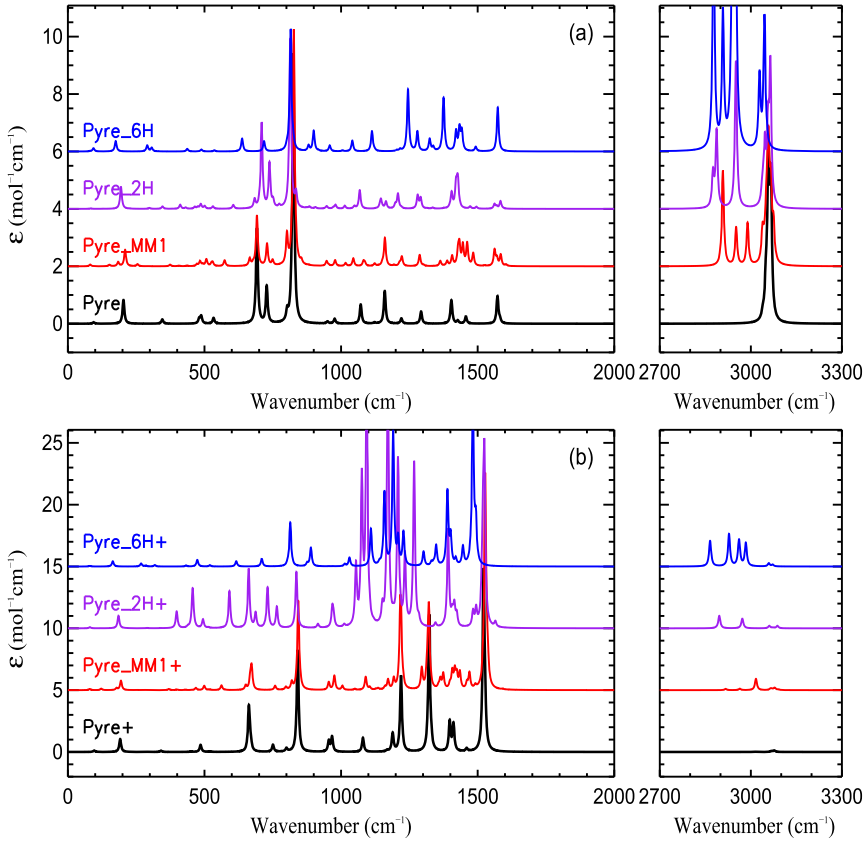

Figure 18. Continued, but for the derivatives of pyrene ("Series D" of Sandford et al. 2013).

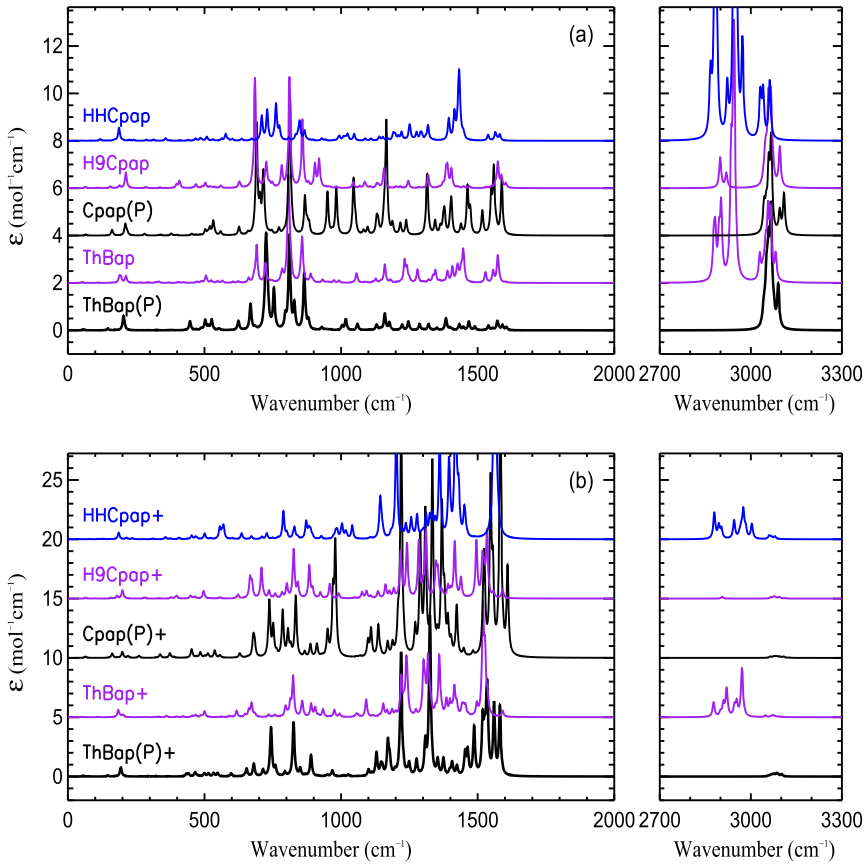

Figure 19. Continued, but for the "Series E" molecules of Sandford et al. (2013).

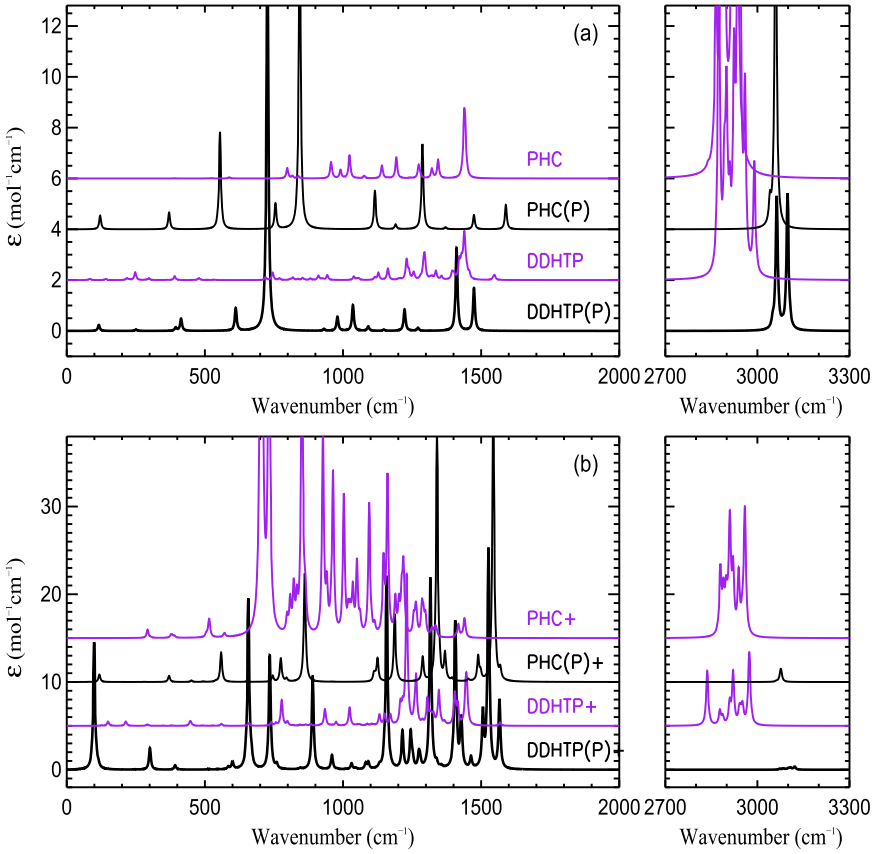

Figure 20. Continued, but for the "Series F" molecules of Sandford et al. (2013).

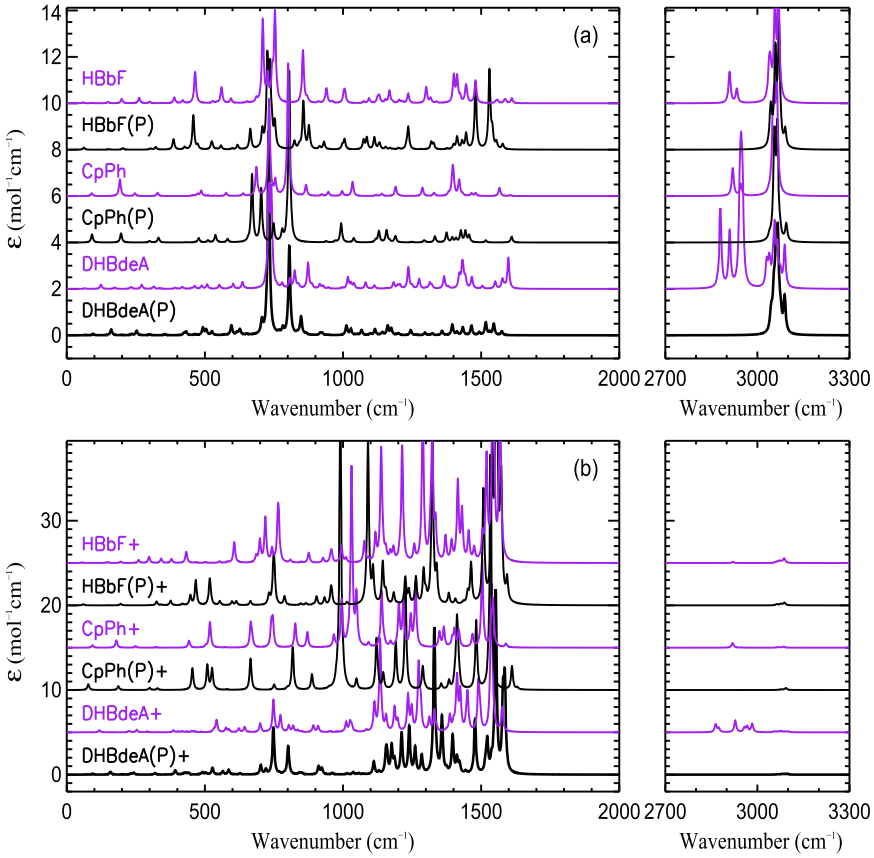

Figure 21. Continued, but for the "Series G" molecules of Sandford et al. (2013).

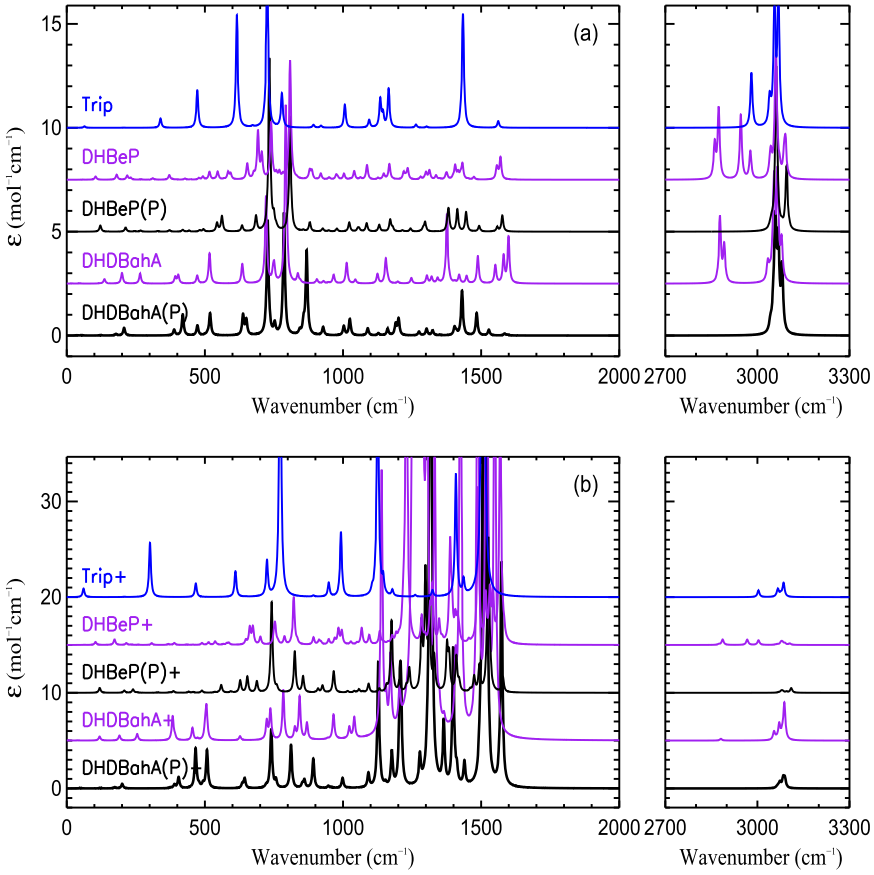

Figure 22. Continued, but for the "Series H" molecules of Sandford et al. (2013).

is presently available, we argue that the relative band strengths derived here are generally reliable.

4. Astrophysical Implications

4.1. Average Spectra

To highlight the features that originated from hydrogenation, we obtain the mean spectra of hydrogenated PAHs, methylated PAHs, and their bare parental compounds, as well as their cationic counterparts (see Figure 24). The mean spectra of hydrogenated PAHs are derived by averaging the computed spectra, on a per aliphatic C–H bond basis, over all the hydrogenated species shown in Figures 1–4, including hydrogenated benzenes, hydrogenated naphthalenes, hydrogenated perylenes, and the hydrogenated molecules of Sandford et al. (2013). For methylated PAHs, we average over all the molecules listed in Figure 2 of Yang et al. (2013). For bare PAHs, we average over benzene, naphthalene, anthracene, phenanthrene, pyrene, perylene, and coronene, the parental molecules of the hydrogenated species shown in Figures 1–4. For both bare PAHs and methylated PAHs, their mean spectra are obtained on a per C atom basis.

As shown in Figure 24, the 3.4 μm feature is clearly seen in the mean spectra of neutral hydrogenated PAHs and of neutral methylated PAHs. Meanwhile, a bump at $\sim$1430 cm^{-1} (which is close to 6.85 μm) is also seen in neutral hydrogenated and methylated PAHs. For hydrogenated neutral PAHs, the average band strengths (per aliphatic C–H bond) are $\langle A_{3.4}\rangle \approx 33.6 \pm 8.8$ km mol^{-1} and $\langle A_{6.85}\rangle \approx 2.59 \pm 1.46$ km mol^{-1} (see Table 9). In contrast, neither the 3.4 μm feature nor the 6.85 μm feature is seen in the spectra of bare PAHs. The mean spectra of hydrogenated PAH ions and of methylated PAH ions also exhibit the aliphatic C–H stretch at 3.4 μm, but this feature is severely suppressed with respect to neutrals. In comparison, cations have much stronger bands than neutrals at $\sim$1200–1600 cm^{-1}. For hydrogenated PAH ions, the average band strengths (per aliphatic C–H bond) are $\langle A_{3.4}\rangle \approx 13.6 \pm 8.7$ km mol^{-1} and $\langle A_{6.85}\rangle \approx 13.2 \pm 13.1$ km mol^{-1} (see Table 9). In the following, we shall focus on the 3.4 and 6.85 μm aliphatic C–H features.

4.2. $A_{3.4}/A_{3.3}$

Figure 25 shows $A_{3.4}/A_{3.3}$, the band-strength ratio of the 3.4 μm aliphatic C–H stretch to the 3.3 μm aromatic C–H stretch computed for all the hydrogenated PAHs and their ions listed in Figures 1–4. For neutral hydrogenated PAHs, the band-strength ratios $A_{3.4}/A_{3.3}$, with an average value of $\langle A_{3.4}/A_{3.3}\rangle \approx 1.98$ and a standard deviation of $\sim$0.60 (see Table 9), do not vary much from one molecule to another. In contrast, $A_{3.4}/A_{3.3}$ varies more appreciably among ions (with $\langle A_{3.4}/A_{3.3}\rangle \approx 7.73$ and a standard deviation of $\sim$6.56; see Table 9), not only for different molecules but also for different isomers of the same molecule. Nevertheless, $A_{3.4}/A_{3.3}$ basically exhibits a low end of $\sim$1.0 for all the cationic hydrogenated PAHs.

4.3. $A_{6.85}/A_{6.2}$

Figure 26 shows $A_{6.85}/A_{6.2}$, the band-strength ratio of the 6.85 μm aliphatic C–H deformation to the 6.2 μm aromatic

Table 8
Same as Table 2 but for the Sandford et al. (2013) Molecules as Shown in Figure 4

Compound	$A_{3.4}$	$A_{6.85}$	$A_{3.3}$	$A_{6.2}$	$A_{3.4}/A_{3.3}$	$A_{6.85}/A_{6.2}$
DHA	18.81	2.01	15.06	0.42	1.25	4.84
HHA	40.15	1.08	29.78	2.37	1.35	0.46
DHPh	28.20	6.11	13.95	0.31	2.02	19.70
DBS	24.06	5.36	15.28	0.38	1.57	14.17
tPHF	39.26	1.32	⋯	⋯	⋯	⋯
DHP	28.04	3.37	15.44	0.46	1.82	7.41
HHP	36.01	2.19	22.31	2.12	1.61	1.03
THBaP	37.64	4.21	14.55	1.73	2.59	2.44
H9CpaP	11.85	3.95	13.80	1.37	0.86	2.89
HHCpaP	34.34	3.29	19.76	0.92	1.74	3.56
DDHTP	39.28	2.15	⋯	0.52	⋯	4.11
PHC	47.18	1.81	⋯	⋯	⋯	⋯
DHBdeA	33.85	3.18	14.31	1.88	2.36	1.69
CpPh	10.55	4.69	15.50	0.48	0.68	9.87
HBbF	12.12	7.23	13.99	1.92	0.87	3.78
DHDBahA	15.35	1.23	13.65	2.75	1.12	0.45
DHBep	29.64	1.61	13.90	1.74	2.13	0.93
TRIP	16.35	⋯	14.05	0.23	1.16	⋯
Average	27.93	3.22	16.35	1.22	1.54	5.15
DHA+	11.44	4.44	3.28	86.14	3.49	0.05
HHA+	34.76	13.82	18.03	261.89	1.93	0.05
DHPh+	4.24	12.78	0.34	30.70	12.60	0.42
DBS+	4.44	55.68	1.85	67.51	2.40	0.82
tPHF+	13.87	3.62	⋯	⋯	⋯	⋯
DHP+	5.70	7.94	0.71	19.55	8.06	0.41
HHP+	9.22	10.69	1.22	20.96	7.55	0.51
THBaP+	17.19	7.71	0.73	12.71	23.47	0.61
H9CpaP+	0.99	0.00	0.66	11.21	1.51	0.00
HHCpaP+	9.75	16.45	2.16	36.04	4.50	0.46
DDHTP+	39.28	12.32	⋯	0.36	⋯	34.72
PHC+	31.47	2.20	⋯	⋯	⋯	⋯
DHBdeA+	10.13	18.24	0.89	19.80	11.37	0.92
CpPh+	3.62	15.03	0.34	17.07	10.67	0.88
HBbF+	0.91	58.14	1.34	54.13	0.68	1.07
DHDBahA+	0.58	2.70	7.19	80.36	0.08	0.03
DHBep+	5.31	14.18	1.16	22.42	4.58	0.63
TRIP+	4.40	⋯	2.68	0.00	1.64	⋯
Average	11.52	15.06	2.84	46.30	6.30	2.77

C–C stretch computed for all the hydrogenated PAHs and their ions listed in Figures 1–4. For the Sandford et al. (2013) molecules, the $A_{6.85}/A_{6.2}$ ratio varies considerably from one molecule to another. Nevertheless, for ∼70% of the Sandford et al. (2013) molecules $A_{6.85}/A_{6.2}$ does not exceed ∼5.0. For the hydrogenated derivatives of neutral benzene and perylene, the $A_{6.85}/A_{6.2}$ ratios are generally in the range of ∼1.0–3.0, with an average value of $\langle A_{6.85}/A_{6.2}\rangle \sim 1.11$ and a standard deviation of ∼0.73. For the hydrogenated cations, the $A_{6.85}/A_{6.2}$ ratios are more scattered than their neutral counterparts, ranging from ∼0.1 to ∼140. However, $A_{6.85}/A_{6.2}$ does not exceed ∼1.0 for ∼82% of the cations. Note that the cations of THN, DHB[de]A, Ben_4H, and Pery_8H_RG2 have a much larger $A_{6.85}/A_{6.2}$ ratio than others, since their C–C stretch modes are significantly suppressed. Finally, if we exclude those molecules with extreme $A_{6.85}/A_{6.2}$ ratios, we derive $\langle A_{6.85}/A_{6.2}\rangle \sim 1.53$ and ∼0.56 for neutrals and cations, respectively, with a standard deviation of ∼1.23 and ∼0.50 (see Table 9).

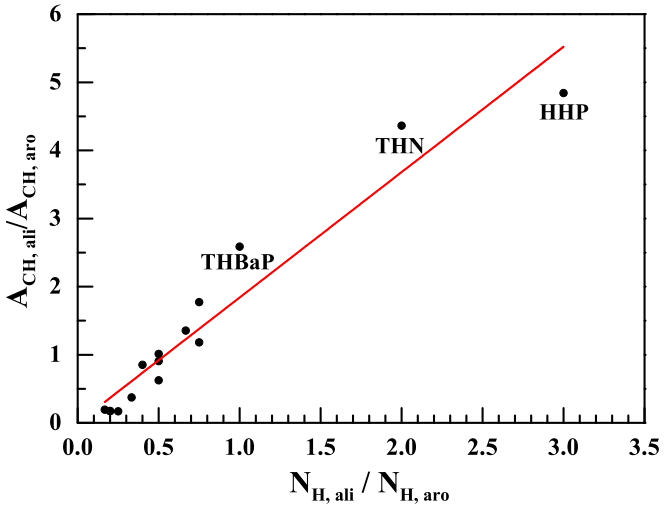

Figure 23. Ratios of the strengths of the 3.4 μm aliphatic C–H stretch ($A_{CH,\,ali}$) to that of the 3.3 μm aromatic C–H stretch ($A_{CH,aro}$) vs. the ratios of the number of aliphatic C–H bonds ($N_{H,ali}$) to the number of aromatic C–H bonds ($N_{H,aro}$) for the Sandford et al. (2013) molecules. The red solid line, with a slope of ∼1.85, is the least-squares fit to the data. The slope would increase to ∼1.98 if the derivatives of benzene, naphthalene, and perylene were also included.

4.4. Degrees of Superhydrogenation

With the computed intrinsic band strength $A_{3.4}/A_{3.3}$, we can estimate the hydrogenation of the UIE carrier. We first make an assumption that the 3.4 μm feature comes exclusively from hydrogenated PAHs. This will place an upper limit on the hydrogenation of the UIE carriers, since those PAHs with aliphatic side groups (e.g., methylated PAHs) and anharmonicity of the aromatic C–H stretch could also contribute to the 3.4 μm feature, sometimes prominently (see Li & Draine 2012).

Let $f_{\rm H} \equiv N_{\rm C,super}/[N_{\rm C,super} + N_{\rm C,arom}]$ be the degree of superhydrogenation, where $N_{\rm C,super}$ is the number of "superhydrogenated" C atoms and $N_{\rm C,arom}$ is the number of aromatic C atoms. Let $I_{3.3}$ and $I_{3.4}$ respectively be the observed intensities of the 3.3 and 3.4 μm emission features. If we assume that one "superhydrogenated" C atom corresponds to two aliphatic C–H bonds[10] and one aromatic C atom corresponds to 3/4 aromatic C–H bonds (intermediate between benzene C_6H_6 and coronene $C_{24}H_{12}$), then $I_{3.4}/I_{3.3} \approx (2/0.75) \times (N_{\rm C,super}/N_{\rm C,arom}) \times (A_{3.4}/A_{3.3})$, i.e., $N_{\rm C,super}/N_{\rm C,arom} \approx 2.67 \times (I_{3.4}/I_{3.3}) \times (A_{3.3}/A_{3.4})$. The degree of superhydrogenation is

$$f_{\rm H} \equiv N_{\rm C,super}/[N_{\rm C,super} + N_{\rm C,arom}] \approx \left[1 + 2.67 \times \frac{I_{3.3}}{I_{3.4}} \times \frac{A_{3.4}}{A_{3.3}}\right]^{-1}, \quad (1)$$

where $A_{3.3}$ and $A_{3.4}$ are measured on a per unit C–H bond basis. Yang et al. (2013) have compiled and analyzed the UIE spectra of 35 sources available in the literature that exhibit both the 3.3 μm and 3.4 μm C–H features. They derived a median ratio of $\langle I_{3.4}/I_{3.3}\rangle \approx 0.12$, with the majority (31/35) of these sources having $I_{3.4}/I_{3.3} < 0.25$ (see Figure 1 of Yang et al. 2013). By

[10] Here we only consider the more normal situation that the extra H is attached to the C atom on the edge of a benzene ring. If the extra H is attached to the C atom in the middle (e.g., the two H atoms shown in the middle of the structure of Naph_10Ha, i.e., c-PHN, in Figure 2), one hydrogenated H atom corresponds to one aliphatic C–H bond.

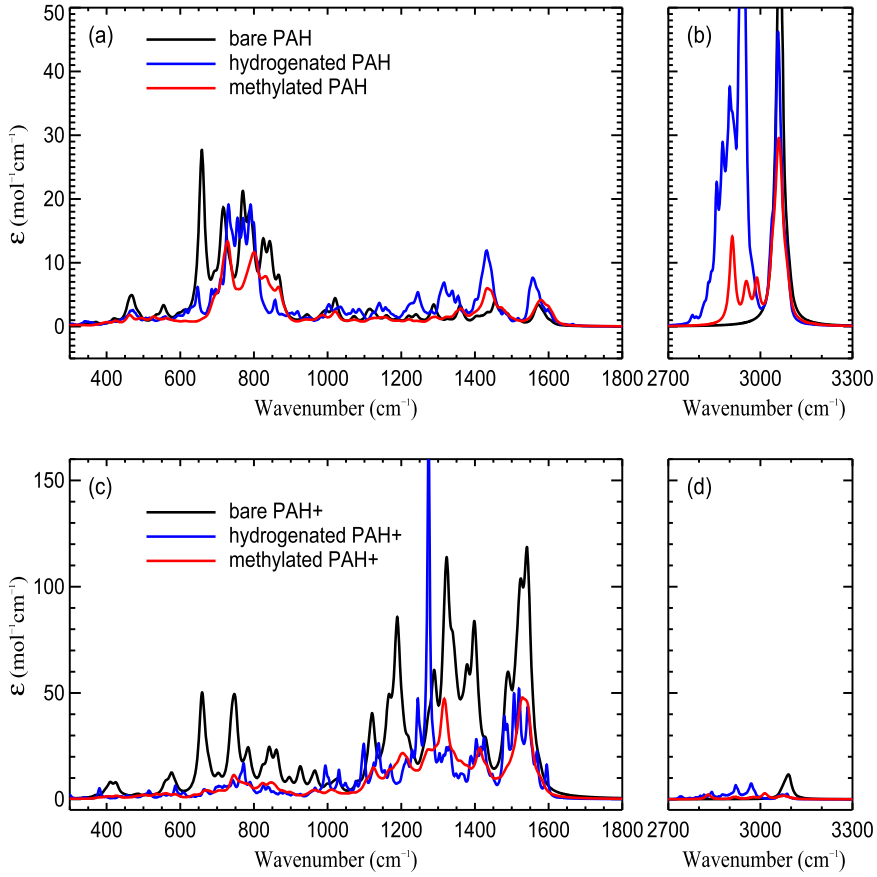

Figure 24. Comparison of the mean spectra of hydrogenated PAHs with methyl PAHs and their bare parental PAHs. The upper panels are for neutrals and the lower panels are for ions. The mean spectra of hydrogenated PAHs are derived by averaging the computed spectra, on a per unit aliphatic C–H bond basis, over all the hydrogenated species shown in Figures 1–4. The mean spectra of methylated PAHs are averaged, on a per C atom basis, over all the molecules listed in Figure 2 of Yang et al. (2013). The mean spectra of bare PAHs are obtained by averaging over benzene, naphthalene, anthracene, phenanthrene, pyrene, perylene, and coronene, on a per C atom basis. For clarity, the mean spectra of methyl PAHs and bare PAHs are scaled by a factor of 2 and 40, respectively.

Table 9

Mean IR Intensities (km mol^{-1}) of the 3.4 and 6.85 μm Aliphatic C–H Bands, the 3.3 μm Aromatic C–H Stretch Band, and the 6.2 μm Aromatic C–C Stretch Band Computed at the B3LYP/6−311+G** Level for All the Hydrogenated Species Shown in Figures 1–4, Including Hydrogenated Benzenes, Hydrogenated Naphthalenes, Hydrogenated Perylenes, and the Hydrogenated Molecules of Sandford et al. (2013)

Compound	$A_{3.4}$	$A_{6.85}$	$A_{3.3}$	$A_{6.2}$	$A_{3.4}/A_{3.3}$	$A_{6.85}/A_{6.2}$
Neutrals	33.62	2.59	16.71	1.87	1.98	3.02[a]
Cations	13.63	13.17	2.69	33.50	7.73	5.19[b]

Notes. The $A_{3.3}$, $A_{3.4}$ and $A_{6.85}$ band strengths are on a per C–H bond basis, while the $A_{6.2}$ band strength is on a per C atom basis. Also tabulated are the band-strength ratios $A_{3.4}/A_{3.3}$ and $A_{6.85}/A_{6.2}$.

[a] $\langle A_{6.85}/A_{6.2}\rangle \approx 1.53 \pm 0.56$ if we exclude those molecules with extreme $A_{6.85}/A_{6.2}$ ratios.

[b] $\langle A_{6.85}/A_{6.2}\rangle \approx 1.23 \pm 0.50$ if we exclude those molecules with extreme $A_{6.85}/A_{6.2}$ ratios.

taking $\langle I_{3.4}/I_{3.3}\rangle \approx 0.12$ and $\langle A_{3.4}/A_{3.3}\rangle \approx 1.98$ for the neutrals and $\langle A_{3.4}/A_{3.3}\rangle \approx 7.73$ for the cations (see Table 9 and Section 4.2), we obtain $f_{\rm H} \approx 2.2\%$ and $\approx$0.57%, respectively. This suggests that the hydrogenation of the UIE emitters is quite small. Note that, as the 3.3 μm feature is predominantly emitted by neutral PAHs, we conclude that, even if the 3.4 μm feature exclusively arises from superhydrogenated PAHs, the degree of superhydrogenation of the UIE carriers would not exceed $\sim$2.2%.

Similarly, if we assume that one "superhydrogenated" C atom corresponds to two aliphatic C–H bonds, the degree of superhydrogenation could also be derived from the 6.85 μm aliphatic C–H deformation band and the 6.2 μm C–C stretch band as follows:

$$f_{\rm H} \approx \left[1 + 2 \times \frac{I_{6.2}}{I_{6.85}} \times \frac{A_{6.85}}{A_{6.2}} \times \frac{B_{6.85}(T)}{B_{6.2}(T)}\right]^{-1}, \qquad (2)$$

where $A_{6.2}$ is measured on a per aromatic C atom basis, $A_{6.85}$ is measured on a per unit C–H bond basis, and $B_{6.2}(T)$ and $B_{6.85}(T)$ are the Planck functions of temperature T at 6.2 and 6.85 μm, respectively. Observationally, detection of the 6.85 μm emission band in the ISM of the Milky Way is much rarer than that of the 3.4 μm emission band. Yang et al. (2016a) have compiled the UIE spectra of Galactic sources that exhibit the 6.85 μm band and found that, except for several Galactic protoplanetary nebulae, the 6.85 μm band is weaker than the 6.2 μm band by a factor of $\gtrsim$10.[11] With $\langle I_{6.85}/I_{6.2}\rangle \lesssim 0.10$ (Yang et al. 2016a), the mean ratio of the observed intensities

[11] For several Galactic protoplanetary nebulae, the 6.85 μm feature is much stronger, with $I_{6.85}/I_{6.2} \gtrsim 1$ for some of these sources (see Yang et al. 2016a; Materese et al. 2017). Such a high $I_{6.85}/I_{6.2}$ ratio is also seen in some protoplanetary nebulae in the Small and Large Magellanic Clouds (see Matsuura et al. 2014; Sloan et al. 2014).

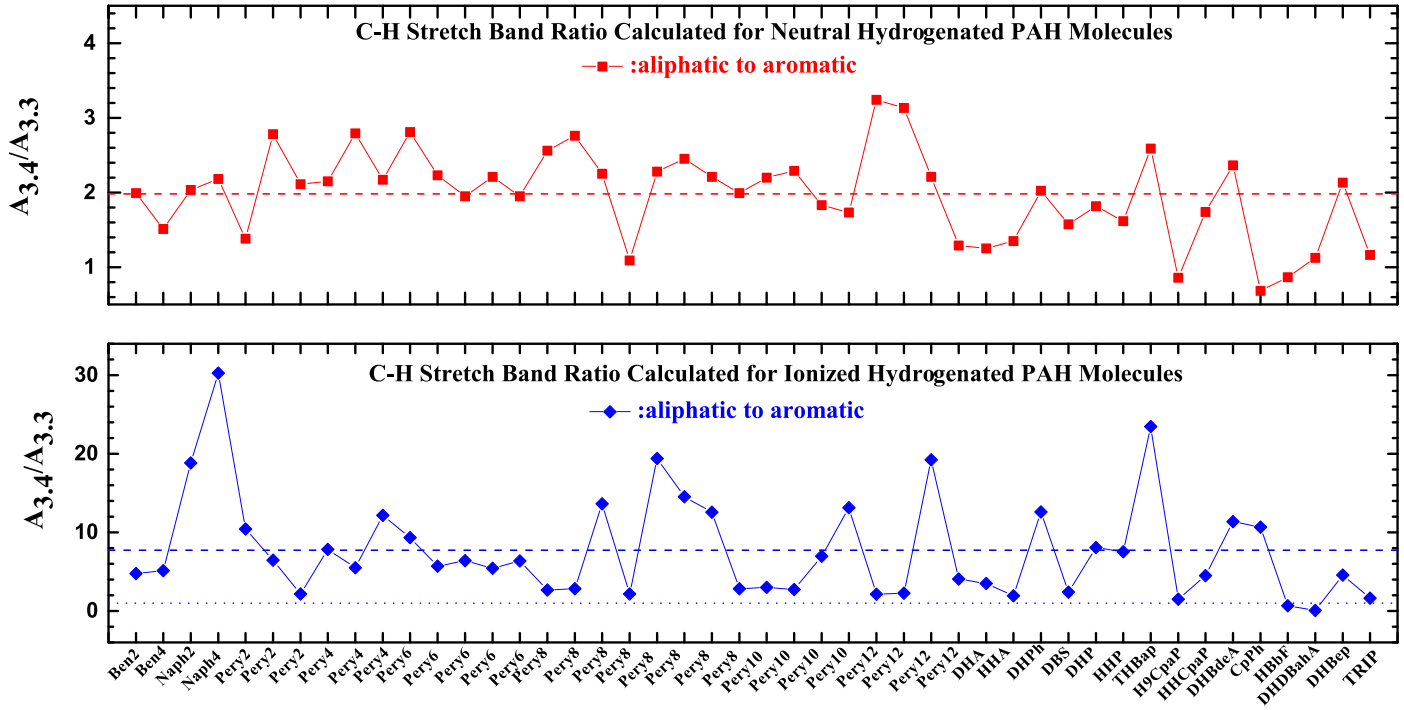

Figure 25. Band-strength ratios ($A_{3.4}/A_{3.3}$) computed at level B3LYP/6−311+G** for the hydrogenated PAH molecules shown in Figures 1–4. The dashed horizontal lines plot the mean value of $\langle A_{3.4}/A_{3.3}\rangle \approx 1.98$ for the neutrals and ≈7.73 for the cations. The dotted horizontal line plots the low-end value of $A_{3.4}/A_{3.3} \gtrsim 1.0$ for all the hydrogenated PAH ions.

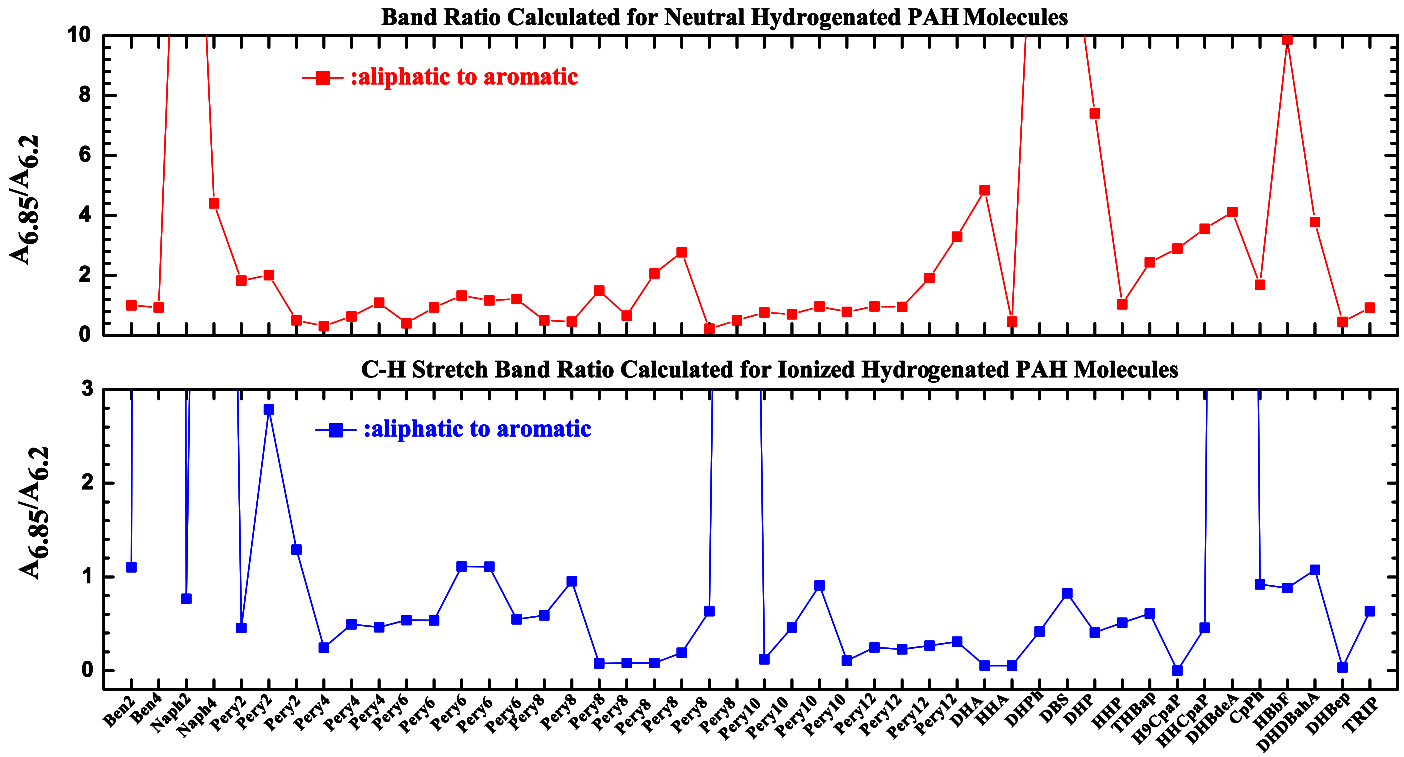

Figure 26. Same as Figure 25 but for $A_{6.85}/A_{6.2}$.

of the 6.85 μm band to the 6.2 μm band, $B_{6.85}/B_{6.2} \approx 1.04 \pm 0.24$ for $200 \lesssim T \lesssim 800$ K (see Yang et al. 2016a), and $\langle A_{6.85}/A_{6.2}\rangle \approx 1.53$ and $\langle A_{6.85}/A_{6.2}\rangle \approx 1.23$, respectively, for the neutrals and cations (see Table 9), we obtain $f_{\rm H} \approx 3.1\%$ and ≈8.6% for the UIE carriers. This also supports the results obtained from the 3.4 μm feature that the superhydrogenation of the UIE carriers is insignificant.

Thanks in large part to the fact that the 3 μm region is accessible to ground-based telescopes, the 3.3 and 3.4 μm bands have been the subject of extensive scrutiny. *ISO* and

AKARI have also provided a wealth of data on these bands. Operating at 5–38 μm, *Spitzer*/IRS unfortunately missed the PAH C–H stretch at 3.3 μm and the accompanying satellite features at 3.4–3.6 μm. Compared with *Spitzer*, *JWST* will have more than an order-of-magnitude increase in sensitivity and spatial resolution, as well as a broader wavelength coverage in the near-IR. It is expected that *JWST*/NIRSpec, operating at 0.6–5 μm, will be able to examine these bands so as to better constrain the degree of superhydrogenation of PAHs and its environmental dependence. The MIRI instrument on board *JWST*, which covers the wavelength range of 5–28 μm, will allow one to extend the mid-IR spectroscopy into new regimes that *ISO* and *Spitzer* could not probe, including the 6.85 and 7.25 μm aliphatic C–H deformation bands in objects, which were too faint for *ISO* and *Spitzer*. Objects of particular interest for exploring the aromatic and aliphatic C–H emission bands include carbon star outflows, protoplanetary nebulae, planetary nebulae, protoplanetary disks around young stars, reflection nebulae, H II regions, PDRs, as well as extragalactic objects (e.g., protoplanetary and planetary nebulae in the Small and Large Magellanic Clouds, the starburst ring of the barred spiral galaxy NGC 1097, and the superwind halo of the prototypical starburst galaxy M82). One would imagine that the 3.4 μm band is more likely to be seen in benign regions. It is puzzling that the 3.4 μm emission is detected in the harsh superwind of M82 and exhibits appreciable enhancements with distance from the galactic plane (see Yamagishi et al. 2012). With the upcoming *JWST*, smaller spatial scales can be probed and spectral mapping in these bands would be valuable for exploring their nature and environmental dependence.

5. Summary

We have used the hybrid DFT method B3LYP in conjunction with the 6–311+G** basis set to compute the IR vibrational spectra of superhydrogenated PAHs and their cations of various sizes (ranging from benzene and naphthalene to perylene and coronene) and of various degrees of hydrogenation (ranging from minimally hydrogenated PAHs to heavily hydrogenated PAHs). For comparison, we have also computed the spectra of monomethylated PAHs as well as their bare parental PAHs. The principal results are as follows:

1. The 3.4 μm aliphatic C–H stretch and the 6.85 μm aliphatic C–H deformation are seen in all these superhydrogenated species, and are more pronounced than in methyl PAHs.
2. For all these superhydrogenated molecules, we have derived from the computed spectra the intrinsic band strengths of the 3.3 μm aromatic C–H stretch ($A_{3.3}$), the 3.4 μm aliphatic C–H stretch ($A_{3.4}$), the 6.2 μm aromatic C–C stretch ($A_{6.2}$), and the 6.85 μm aliphatic C–H deformation ($A_{6.85}$). By averaging over all these molecules, for hydrogenated neutral PAHs we have determined the mean band strengths (per aliphatic C–H bond) of $\langle A_{3.4}\rangle \approx 33.6$ km mol^{-1} and $\langle A_{6.85}\rangle \approx 2.59$ km mol^{-1}, and the mean band-strength ratios of $\langle A_{3.4}/A_{3.3}\rangle \approx 1.98$ and $\langle A_{6.85}/A_{6.2}\rangle \approx 1.53$. For hydrogenated PAH cations, the corresponding band strengths and band-strength ratios are $\langle A_{3.4}\rangle \approx 13.6$ km mol^{-1} and $\langle A_{6.85}\rangle \approx 13.2$ km mol^{-1}, and $\langle A_{3.4}/A_{3.3}\rangle \approx 7.73$ and $\langle A_{6.85}/A_{6.2}\rangle \approx 0.56$.
3. By comparing the computationally derived mean ratio of $\langle A_{3.4}/A_{3.3}\rangle \approx 1.98$ with the mean ratio of the observed intensities $\langle I_{3.4}/I_{3.3}\rangle \approx 0.12$, we have estimated the degree of superhydrogenation to be only $\sim$2.2% for the neutral PAHs, which predominantly emit the 3.3 and 3.4 μm features. We have also derived the degree of superhydrogenation from the mean ratio of the observed intensities $\langle I_{6.85}/I_{6.2}\rangle \lesssim 0.10$ and $\langle A_{6.85}/A_{6.2}\rangle \approx 1.53$ for neutrals and $\langle A_{6.85}/A_{6.2}\rangle \approx 0.56$ for cations to be $\lesssim$3.1% for neutrals and $\lesssim$8.6% for cations. The actual degrees of superhydrogenation could be even lower since methylated PAHs and the anharmonicity of PAHs could also contribute to the observed 3.4 and 6.85 μm aliphatic C–H bands. Therefore, we conclude that astrophysical PAHs are primarily aromatic and are not significantly superhydrogenated.

We thank the anonymous referee for his/her very helpful comments and suggestions. X.J.Y. is supported in part by NSFC 11873041 and the NSFC-CAS Joint Research Funds in Astronomy (U1731106, U1731107). A.L. is supported in part by NASA grant 80NSSC19K0572. R.G. is supported in part by NSF-PRISM grant Mathematics and Life Sciences (0928053). Computations were performed using the high-performance computer resources of the University of Missouri Bioinformatics Consortium.

References

Acke, B., Bouwman, J., & Juhász, A. 2010, ApJ, 718, 558
Allamandola, L. J., Hudgins, D. M., & Sandford, S. A. 1999, ApJ, 511, 115
Allamandola, L. J., Tielens, A. G. G. M., & Barker, J. R. 1985, ApJL, 290, L25
Allamandola, L. J., Tielens, A. G. G. M., & Barker, J. R. 1989, ApJS, 71, 733
Andrews, H., Candian, A., & Tielens, A. G. G. M. 2016, A&A, 595, 23
Bakes, E. L. O., & Tielens, A. G. G. M. 1994, ApJ, 427, 822
Barker, J. R., Allamandola, L. J., & Tielens, A. G. G. M. 1987, ApJL, 315, L61
Bauschlicher, C. W., Jr. 1998, ApJL, 509, L125
Bernstein, M. P., Sandford, S. A., & Allamandola, L. J. 1996, ApJL, 472, L127
Borowski, P. 2012, JPCA, 116, 3866
Boschman, L., Reitsma, G., Cazaux, S., et al. 2012, ApJL, 761, L33
Brenner, J., & Barker, J. R. 1992, ApJL, 388, L39
Cassam-Chenaï, P., Pauzat, F., & Ellinger, Y. 1994, AIPC, 312, 543
Cazaux, S., Boschman, L., & Rougeau, N. 2016, NatSR, 6, 19835
Chen, T., Luo, Y., & Li, A. 2019, A&A, 632, A71
Draine, B. T., & Li, A. 2001, ApJ, 551, 807
Frisch, M. J., Trucks, G. W., Schlegel, H. B., et al. 2009, Gaussian, Inc 09, Revision B01 (Wallingford, CT: Gaussian, Inc)
Geballe, T. R., Joblin, C., d'Hendecourt, L. B., et al. 1994, ApJL, 434, L15
Geballe, T. R., Lacy, J. H., Persson, S. E., McGregor, P. J., & Soifer, B. T. 1985, ApJ, 292, 500
Geballe, T. R., Tielens, A. G. G. M., Allamandola, L. J., Moorhouse, A., & Brand, P. W. J. L. 1989, ApJ, 341, 278
Goto, M., Usuda, T., Takato, N., et al. 2003, ApJ, 589, 419
Halasinski, T. M., Salama, F., & Allamandola, L. J. 2005, ApJ, 628, 555
Hammonds, M., Pathak, A., & Sarre, P. J. 2009, PCCP, 11, 4458
Jensen, P., A. m Leccese, M., Simonsen, F. D. S., et al. 2019, MNRAS, 486, 5492
Joblin, C., d'Hendecourt, L., Léger, A., & Defourneau, D. 1994, A&A, 281, 923
Joblin, C., Tielens, A. G. G. M., Allamandola, L. J., & Geballe, T. R. 1996, ApJ, 458, 610
Jourdain de Muizon, M., d'Hendecourt, L. B., & Geballe, T. R. 1990, A&A, 235, 367
Jourdain de Muizon, M., Geballe, T. R., d'Hendecourt, L. B., & Baas, F. 1986, ApJL, 306, L105
Klærke, B., Toker, Y., Rahbek, D. B., Hornekær, L., & Andersen, L. H. 2013, A&A, 549, 84
Kondo, T., Kaneda, H., Oyabu, S., et al. 2012, ApJL, 751, L18
Léger, A., & Puget, J. 1984, A&A, 137, L5
Le Page, V., Snow, T. P., & Bierbaum, V. M. 2009, ApJ, 704, 274
Li, A., & Draine, B. T. 2012, ApJL, 760, L35
Maltseva, E., Mackie, C. J., Candian, A., et al. 2018, A&A, 610, 65
Maltseva, E., Petrignani, A., Candian, A., et al. 2016, ApJ, 831, 58
Materese, C. K., Bregman, J. D., & Sandford, S. A. 2017, ApJ, 850, 165

Matsuura, M., Bernard-Salas, J., Lloyd Evans, T., et al. 2014, MNRAS, 439, 1472
Nagata, T., Tokunaga, A. T., Sellgren, K., et al. 1988, ApJ, 326, 157
Pauzat, F., & Ellinger, Y. 2001, MNRAS, 324, 355
Peeters, E., Allamandola, L. J., Hudgins, D. M., Hony, S., & Tielens, A. G. G. M. 2004, in ASP Conf. Ser. 309, Astrophysics of Dust, ed. A. N. Witt, G. C. Clayton, & B. T. Draine (San Francisco, CA: ASP), 141
Quitián-Lara, H. M., Fantuzzi, F., Nascimento, M. A. C., et al. 2018, ApJ, 854, 61
Rasmussen, J. A., Henkelman, G., & Hammer, B. 2011, JChPh, 134, 164703
Rauls, E., & Hornekær, L. 2008, ApJ, 679, 531
Ricks, A. M., Douberly, G. E., & Duncan, M. A. 2009, ApJ, 702, 301
Sandford, S. A. 1991, ApJ, 376, 599
Sandford, S. A., Allamandola, L. J., Tielens, A. G. G. M., et al. 1991, ApJ, 371, 601
Sandford, S. A., Bernstein, M. P., & Materese, C. K. 2013, ApJS, 205, 8
Schutte, W. A., Tielens, A. G. G. M., & Allamandola, L. J. 1993, ApJ, 415, 397
Seok, J. Y., & Li, A. 2017, ApJ, 835, 291
Sloan, G. C., Bregman, J. D., Geballe, T. R., Allamandola, L. J., & Woodward, C. E. 1997, ApJ, 474, 735
Sloan, G. C., Lagadec, E., Zijlstra, A. A., et al. 2014, ApJ, 791, 28
Smith, T. L., Clayton, G. C., & Valencic, L. 2004, AJ, 128, 357
Steglich, M., Jäger, C., Huisken, F., et al. 2013, ApJS, 208, 26
Thrower, J. D., Friis, E. E., Skov, A. L., et al. 2014, PCCP, 16, 3381
Thrower, J. D., Jørgensen, B., Friis, E. E., et al. 2012, ApJ, 752, 3
Tielens, A. G. G. M. 2008, ARA&A, 46, 289
Wagner, D. R., Kim, H., & Saykally, R. J. 2000, ApJ, 545, 854
Weingartner, J. C., & Draine, B. T. 2001, ApJS, 134, 263
Wolf, M., Kiefer, H. V., Langeland, J., et al. 2016, ApJ, 832, 24
Yamagishi, M., Kaneda, H., Ishihara, D., et al. 2012, A&A, 541, A10
Yang, X. J., Glaser, R., Li, A., & Zhong, J. X. 2013, ApJ, 776, 110
Yang, X. J., Glaser, R., Li, A., & Zhong, J. X. 2016a, MNRAS, 462, 1551
Yang, X. J., Glaser, R., Li, A., & Zhong, J. X. 2017a, NewAR, 77, 1
Yang, X. J., Li, A., Glaser, R., & Zhong, J. X. 2016b, ApJ, 825, 22
Yang, X. J., Li, A., Glaser, R., & Zhong, J. X. 2017b, ApJ, 837, 171